Journal of *Marine Science and Engineering*

MDPI

Article

Spatio-Temporal Trend of Past and Future Extreme Wave Climates in the Gulf of Guinea Driven by Climate Change

Adeola M. Dahunsi [1,*], Frédéric Bonou [1,2,3], Olusegun A. Dada [4] and Ezinvi Baloïtcha [1]

[1] International Chair in Mathematical Physics and Applications (UNESCO-ICMPA Chair), Faculty of Sciences and Technologies (FAST), University of Abomey-Calavi, Cotonou 01 BP 526, Benin
[2] Laboratoire de Physiques et Applications LHA, Université Nationale des Sciences, Technologie, Ingénierie et Mathématiques (UNSTIM), Abomey BP 2282, Benin
[3] Laboratoire d'Hydrologie Marine et Côtiére, Intitut de Recherches Halieutiques et Océanologiques du Bénin, Cotonou 03 BP 1665, Benin
[4] Department of Marine Science and Technology, Federal University of Technology, Akure 340252, Nigeria
* Correspondence: dahunsi.adeola@yahoo.com or dahunsi_adeola_michael@cipma.net

Abstract: This study assessed the extremes of wave conditions for past (1979–2005) and future (2026–2045 and 2081–2100) time slices in the Gulf of Guinea (GoG). The ensemble produced from eight General Circulation Models under different Representative Concentration Pathway (RCP) emission scenarios (RCP4.5 and RCP8.5) was subjected to linear regression analysis and Mann–Kendal test for their trends and significance, respectively. Results showed an increase in the extreme of significant wave height (*Hs*) and mean wave period (*Tm*) between 1979–2005, 2026–2045, and 2081–2100 with few exceptions. The average values of annual and seasonal *Hs* and *Tm* range from 1.26–1.62 m and 10.37 s–10.86 s, respectively, for 1979–2005. These *Hs* values are projected to increase by 0.1 m (0.05 m) to 1.72 m (1.67 m) and the *Tm* will increase by 0.29 s (0.24 s) to 11.15 s (11.10 s) by the end of the century (mid-century) time slices, respectively. The mean wave direction (*Dm*) (201.89°–206.27°) showed an anticlockwise shift (-29.2×10^{-3} degrees per year) for 1979–2005 which is projected to become more southwesterly with an increase up to 2.2° (0.5°) by end (mid) century in 2100 (2045), respectively. Future work will be on the impacts of changing wave on longshore sediment transport along the GoG.

Keywords: Gulf of Guinea; extreme wave climate; climate change; ensemble; RCP; Mann–Kendal

Citation: Dahunsi, A.M.; Bonou, F.; Dada, O.A.; Baloïtcha, E. Spatio-Temporal Trend of Past and Future Extreme Wave Climates in the Gulf of Guinea Driven by Climate Change. *J. Mar. Sci. Eng.* **2022**, *10*, 1581. https://doi.org/10.3390/jmse10111581

Academic Editor: Mustafa M. Aral

Received: 31 August 2022
Accepted: 11 October 2022
Published: 26 October 2022

1. Introduction

Wind-generated waves (hereafter called "waves") can be of two types depending on their point of generation. They can be classified as either ocean swells that are generated offshore or wind seas that are generated locally close to the coast [1]. Waves are generally very important because they play a key role in several coastal engineering and marine environmental studies. These influences can be seen both in the open ocean and coastal areas in the forms of flooding, coastal erosion, risks to offshore activities and structures as well as maritime transportation [2]. Waves also have a very vital influence on global climate in that it modifies the exchange of momentum, heat, and mass across the atmosphere–ocean interface [3].

Trends of average and extreme wave climate have been known to have remarkable impacts on marine as well as coastal activities and their dependent industries such as shipping and offshore oil rigs. Several other ocean dynamics, in addition to the changing trends of wave climate, are directly or indirectly affected by climate change. These global warming impacts, such as sea level rise [4], all contribute to exacerbating coastal problems such as flooding [5–8] and erosion [9–11]. Due to the impacts of climate change on variables, such as winds, driving the generation and propagation of surface waves, changes in wave

climate are expected globally [12]. These impacts are expected to also result in changes in wave energy and its reach of impacts [6].

The designs of coastal and offshore structures require a good understanding of extreme oceanic phenomena, such as waves, to increase their effectiveness and durability. Information on severe wave conditions such as significant wave height (*Hs*), which are derived by estimating extreme *Hs* for different return periods, is also very vital in the design of ships because it gives a hint of the estimated life expectancy of the ships under extreme wave conditions [13]. These applications of information on extreme wave conditions are not only limited to core engineering cases such as coastal engineering [14], assessment of vulnerability to a coastal hazard [15], siting of renewable energy facilities [16] but they are also very important in more biological studies such as an assessment of marine habitat distribution [17]. This is especially important for a region such as the Atlantic Gulf of Guinea (GoG), where the productivity of the coastal upwelling region is very important for sustaining the livelihoods of several coastal dwellers.

The GoG is a part of the West African upwelling system popularly referred to as the Guinea Current Large Marine Ecosystem (GCLME) reported to be one of the largest marine ecosystems globally [18]. It provides a home to a high percentage of the region's fisheries and aquaculture because of the high nutrient inputs from coastal sources and upwelling [19,20]. One of the most important economic activities in some countries in the GoG is crude oil exploration, which is the major source of foreign exchange for countries such as Nigeria [21,22]. This offshore and onshore oil exploration warrants the installation of marine and coastal engineering structures whose efficiency and durability depend on the understanding of the extremes of wave climate in the GoG [14]. According to the World Bank report [23], more than 30% of the population of West Africa lives in the coastal areas. This shows that a great percentage of the dwellers of the region is vulnerable to the impact of climate change on wave conditions.

This aforementioned vulnerability coupled with the fact that there is no existing database for wave observation in the region stresses the need for close monitoring of the wave changes in the region through improved observation and modeling. Wave data from observation or in situ measurements, such as buoys and radar, are the most accurate data because of their high temporal resolution. However, they have a poor spatial resolution in some regions of the global ocean due to their sparse distribution. The GoG is one of such regions where one can hardly find wave monitoring buoys data, making such sources poor sources of historical data for the region. Data for wave studies come from various other sources including voluntary observing ships (VOS) [24–26], wave model reanalysis data [27–29] as well as Satellite altimetry [30]. As a result of their ability to provide past and future data for remote areas, wave data from the models serve as the ideal data source for assessing long-term historical and future wave climates in relatively unmonitored parts of the global ocean such as the GoG. This is owing to their relatively cheap cost and efficiency in simulating wave conditions for the past, present, and future.

Though good for assessing the general trend of the average condition of wave climate, global studies such as the assessment of global changes in wave climate based on a multi-model ensemble conducted by [29], 21st century global projections by [12] and global uncertainties modeling in [31] are unable to properly represent the local spatial variations in regional wave climate. Studies assessing the future trends of wave climate have been performed in several parts of the global ocean such as the Northeast Atlantic Ocean [32], the Mediterranean [33], the Northwest Mediterranean Sea [34], East China Sea [35] and Indian Ocean [2]. However, previous studies in the GoG such as [22,36,37] have only assessed the past extreme of wave conditions. This is because in the past, assessing the future trends of wave climate was not possible in regions such as the Gulf of Guinea due to the unavailability of global ocean wave climate projections. This problem was recently overcome through the Coordinated Ocean Wave Climate Projection (COWCLIP) project [38–40]. This project has led to the development of global wave climate projections for different time slices covering the past and future [39]. The need for regional assessment of the past and future trends

of extreme wave conditions, as noted by [2], is very important to inform effective coastal management in vulnerable regions such as the GoG, which is part of the goals of this study.

The present study seeks to assess the past and future trends of extreme wave climate using an ensemble produced from eight General Circulation Models (GCMs)-derived wave datasets from the COWCLIP project. This will provide a clearer picture of the regional conformity or deviations from the global trends since all previously mentioned studies have observed strong regional deviations from projected global trends of wave climate.

2. Description of the Study Area

The GoG, which includes the Island States of Sao Tome and Principe, extends from Cape Palmas in Liberia (northwest) to Cape Lopez in Gabon (southeast) (P46 and P1, respectively). For this study, the GoG has been defined as regions between longitudes 7.5° W–15° E and latitudes 15° N–1.5° S. Its coastal area consists of sandy beaches [41], rocky shores [21], mud coasts [42] as well as deltas such as Niger and Volta [43] along its stretch.

The continental shelf of the GoG is narrow [44] and it is a swell-dominated region [45]. The region has many rivers flowing into the Atlantic Ocean, and the prominent ones are the Sassandra, Bandama, Comoé, Volta, Mono, Oueme, and Niger rivers. They are the major sources of sediments on the coasts [46]. The predominant type of wave experienced in the study area is the ocean swell generated by storms from the southwestern part of the Atlantic Ocean [45,47]. The GoG is a very important region to the economy of the West African sub-region because it contributes more than half of the Gross Domestic Product of the countries in this part of the world [46]. This is because its continental shelf contains deposits of crude oil and gas in locations such as the Espoir oil field between Coté d'Ivoire and Ghana, the Lomé oil field between Ghana and the Benin Republic, and the Aje oil field in the Niger Delta, Nigeria [22].

For the assessment of the extreme conditions of the wave climate in this study, 46 points, starting from P1 in Gabon in the southeast to P46 in Cote d'Ivoire in the northwest labeled P1-P46 (Figure 1) have been selected on the coastline of the GoG. The selection of points P1-P46 is based on the even distribution of the points and the availability of data close to the points. This even distribution will make it easier to observe local spatial variations in wave climate that may occur in the countries located in the GoG region, thereby, giving a clearer evolution of the regional and local trends in wave conditions.

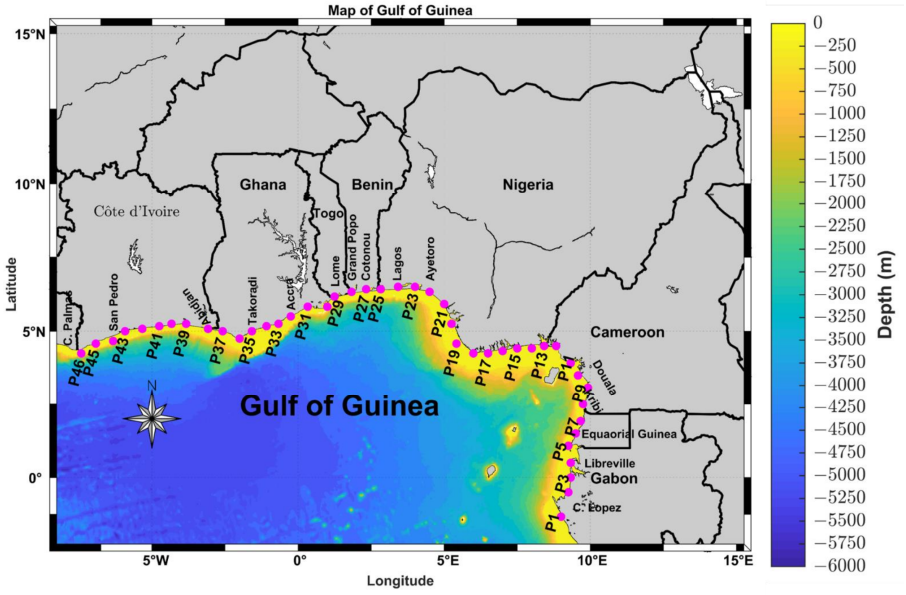

Figure 1. Map of the Gulf of Guinea arm of the Atlantic Ocean with the selected points P1–P46. Blue = deep ocean, yellow = coastal water/continental shelf.

3. Data and Methods

3.1. Datasets

In this study, the COWCLIP2.0 GCMs-derived wave [38,39] datasets (hereafter referred to as CP-GCM) were used. The CP-GCM data, produced under the second phase of the COWCLIP, consisting of about 155 simulations of wave conditions on a global scale, is forced using wind fields from 10 Coupled Model Intercomparison Project 5 General Circulation Models (CMIP5 GCMs). This open-access dataset comprises both dynamically and statistically simulated wave data. For the present study, the contribution of the Commonwealth Scientific and Industrial Research Organisation (CSIRO) to the COWCLIP2.0 project, i.e., the CSIRO multiple-model multiple-scenario ensemble was used [1,39,48]. It consists of WAVEWATCH III (WW3) dynamically simulated wave data using 10 m above surface wind field forcing from 8 CMIP5 GCMs (Table 1). The model setup for the generation of this globally available dataset made use of the ST3 (BAJ) source term physics in WW3. The details of the WW3 setup for this dataset simulation are provided in the previous studies [12,39]. The database consists of various time slices representing the historical (1979–2005), the mid-century (2026–2045) and the end-century (2081–2100). The future projections are also available for two Representative Concentration Pathway (RCP) emission scenarios, i.e., RCP4.5 and RCP8.5 which are all analyzed in this study. According to [49,50], RCP4.5 and RCP8.5 are some of the representative concentration pathways included in the Fifth Assessment Report of IPCC (AR5) [51]. They signify the greenhouse gas (GHG) emission scenarios with a projected radiative forcing of 4.5 Wm^{-2} and 8.5 Wm^{-2} by the end of the century in 2100, respectively. While the RCP8.5 scenario represents the scenarios releasing high GHG into the environment, the RCP4.5 represents the scenario where efforts are made to stabilize the climate by adopting technologies and climate change mitigation and adaptation strategies before the end of the 21st century.

Table 1. CMIP5 GCMs from CSIRO-COWCLIP2.0 used for this study.

S/N	GCM	Model Full Name
1	ACCESS1.0	Australian Community Climate and Earth System Simulator 1.0
2	BCC-CSM1.1	Beijing Climate Centre, Climate System Model, 1-1
3	CNRM-CM5	Centre National de Recherches Meteorologiques Coupled Global Climate Model, version 5
4	GFDL-CM3	Geophysical Fluid Dynamics Laboratory Climate Model 3
5	HadGEM2-ES	Hadley Centre Global Environmental Model 2, Earth System
6	INM-CM4	Institute of Numerical Mathematics Coupled Model, version 4.0
7	MIROC5	Model for Interdisciplinary Research on Climate, version 5
8	MRI-CGCM3	Meteorological Research Institute Coupled Atmosphere-Ocean General Circulation Model, version 3

The extreme wave parameters extracted from both CP-GCM were the 99th percentile of significant wave height (*Hs*), the mean wave period (*Tm*), and mean wave direction (*Dm*). The CP-GCM data are a gridded dataset provided on a monthly, seasonally, and annually basis but the monthly average was extracted for this study. This is to enable the definition of the seasons based on the two dominant seasons in the GoG rather than the four in some parts of the world. The model data has a spatial resolution of $1^\circ \times 1^\circ$ and was further downscaled to $0.5^\circ \times 0.5^\circ$ to increase the chance of having data closer to points of interest on the coast. This was performed using the linear interpolation method which is based on the principle of triangulation thereby interpolating the nearest available grid points around the interpolated data points. The datasets consist of the historical time slice which covers a period of 27 years between 1979–2005 while the future time slices are 20 years for the mid-century (2026–2045) and end-century (2081–2100) for both RCP 4.5 and RCP 8.5. The extracted data covered 15° N–1.5° S and 7.5° W–15° E which include the coastal area of the GoG and its surrounding continental shelf water.

The data from 8 GCMs, as shown in Table 1 (ACCESS1-0, BCC-CSM1-1, CNRM-CM5, GFDL-CM3, HadGEM2-ES, INM-CM4, MIROC5, and MRI-CGCM3), were used to produce an ensemble for the 3 bulk parameters *Hs*, *Tm*, and *Dm* used in this study. The ensemble

was produced by finding the average of the wave parameters from the other 8 GCMs. The ensemble was chosen for further analysis in assessing the extreme wave conditions in the GoG because it is believed to be more representative of all the models and encourages comparison with previous studies that have used a similar approach [45]. The data points from the gridded data nearest to the preselected points on the coast were interpolated to the coast for further analysis.

3.2. Selection of Coastal Points

The 46 points (P1-P46) selected as locations for analysis of extreme wave climate in this study were defined in terms of longitude and latitudes to have relatively even distribution. They are points near or coinciding with already digitized coordinates included in the Global Self-consistent, Hierarchical, High-resolution Geography (GSHHG) database that fall between longitudes 7.5° W–15° E and latitudes 15° N–1.5° S. The first condition for selection was that the points must coincide with locations that are easily identifiable on Google Earth. This condition guaranteed that all economically important locations especially the big cities of the countries (e.g., Abidjan, Accra, Lomé, Cotonou and Lagos, Dakar, etc.), in the GoG are selected. Points of significant hydrodynamics activities in the region (e.g., Ayetoro, Takoradi, San-Pedro, Kribi, etc.), are further selected. Afterward, even distribution of points in-between these other locations was completed. This is to enable capturing the average local changes in wave conditions in different parts of the GoG. As a swell-dominated region, the coastal wave conditions in the GoG reflect changes in offshore wave conditions. The narrow continental shelf seen in most places in the GoG allows the wave from the southwest Atlantic to travel far nearshore with little changes due to bathymetry. A similar trend was found by [52] for the narrow continental shelf of North Carolina where the offshore wave shows a very low difference with conditions nearshore due to the weak influence of local wind waves. Finally, coastal points selections were then subjected to further elimination of overlapping points (too close points) for clarity of figures. The coordinates of the resulting 46 selected points are given in the Supplementary Materials Table S1.

3.3. Extreme Wave Climate Analysis

The extreme wave conditions are defined to be the 99th percentile which can be referred to as the maximum values for all wave parameters [22]. This approach was adopted, instead of defining a particular threshold for the extreme wave climate, due to variations in the wave parameters in the GoG. Since it has been employed in previous studies including [22,36], it will aid in intercomparison and confirmation of results. The analysis was completed on an annual as well as seasonal basis. Since there are two major seasons in the GoG: wet (boreal summer) and dry (boreal winter); the duration of each of the two seasons is 7 months and 5 months, respectively, similar to previous studies in the GoG. The months of the wet season, hereafter refer to as summer, are from April–October while the months of the dry season, hereafter refer to as winter, are from November–March.

The bulk wave parameters for the 46 selected points were extracted from the ensemble dataset by finding the nearest data point to predefined points on the coast. The annual analysis was completed by finding the average of the extreme wave parameters for all the years. The seasonal analysis was completed similarly after grouping all the months into their respective seasons. The averages and trends of the extreme *Hs*, *Tm*, and *Dm* were estimated and presented in Section 4.

3.4. Trends and Changes in Extreme Wave Conditions

For the past time slice, to assess the rates of change in the extreme wave conditions previously estimated, trend analysis was carried out for each parameter on an annual and seasonal basis. To carry out trend analysis for this study, a linear regression approach was employed. This was performed using the same approach employed in the "Trend function"

of the climate toolbox [53]. This involves fitting a polynomial, p of degree 1 to each of the grid points used in the time dimension of the matrix.

To assess the change that is projected to occur between the past and the future time slices under the different climate change scenarios, the differences between the past and future average wave conditions at each selected point were calculated for the various climate change RCP scenarios. This was estimated using simple subtraction as shown in Equation (1):

$$\text{Changes} = \text{X\_future} - \text{X\_past} \quad (1)$$

where X = wave climate such as *Hs*, *Tm* or *Dm*, X_future = wave condition for the future time slices (2026–2045 and 2081–2100), X_past = wave condition for the past time slice (1979–2005).

3.5. Statistical Tests of Significance

For the historical time slice, after the trend analysis was done, a Mann–Kendall test was carried out to check the existence of a significant trend in the extreme conditions of the wave parameters on annual and seasonal bases. The MATLAB statistical function, "mann_kendall", included in the climate data toolbox by [53] was used for this test. This function mann_kendall performs a Mann–Kendall test to ascertain the significance of the trend estimated by the other function named "trend" mentioned in the previous section. This test has the null hypothesis defined as the absence of a trend in the parameter being tested, in this case, the extreme wave conditions. The alternative hypothesis, therefore, is that the trend is statistically significant. For this study, the default alpha significance level of 95% was used. The result interpretation was performed in a way that when the *p*-value derived from the test is lower than alpha, the null hypothesis is rejected whereas when the *p*-value is higher than alpha, it means there is no sufficient evidence to reject the null hypothesis [54–56].

In order to check the existence of a statistically significant difference between the mid-century and end-century future time slices, a combination of one-way analysis of variance (ANOVA) and Tukey–Kramer test was performed. The ANOVA test was performed using the "anova1" function in MATLAB which is used to test the null hypothesis that the wave climate from the various RCP scenarios for all future time slices have an equal mean against the alternative hypothesis that at least one of the RCP scenarios has a different mean. This was followed by the Tukey–Kramer test which is an honestly significant differences test to see which of the RCP scenarios has a different mean. The tests were carried out at a confidence interval with alpha = 0.05 to check for the F-value and *p*-value at a 95% confidence level. The resulting output, presented in Section 4, is interpreted as a test showing *p*-value higher than the defined alpha value signifies insufficient evidence to conclude that there is a statistically significant difference between the RCP scenarios being tested. Additionally, the lower the F-value, the higher the evidence that there is no statistically significant difference between the means of the RCP scenarios.

4. Results

4.1. Past Extreme Wave Climate and Trends

The results of the analysis completed on the historical time slice 1979–2005 for *Hs*, *Tm*, and *Dm* are presented in this subsection in terms of annual, winter, and summer averages as well as the rate of change in the parameters for the years covered.

The spatial distribution of extreme *Hs* presented in Figure 2a–c shows that the extreme *Hs* in GoG has a relatively uniform distribution close to the coast. Although a closer observation shows higher values (up to 2 m) in the western part around Cote d'Ivoire labeled P46 on the study area map in Figure 1. These little variations show reduction eastward which is most noticeable around P14 in the Nigerian Niger Delta with *Hs* as low as 0.5 m. This region of exceptionally low *Hs* continues through Cameroon down to P5 in Equatorial Guinea where another southward increase can be seen down to Gabon. These slight west-to-east decreasing trends are observed on both seasonal and annual bases. The

orientation of the wave roses shows the direction of incidence of the waves in various bins represented by the values on the color bar.

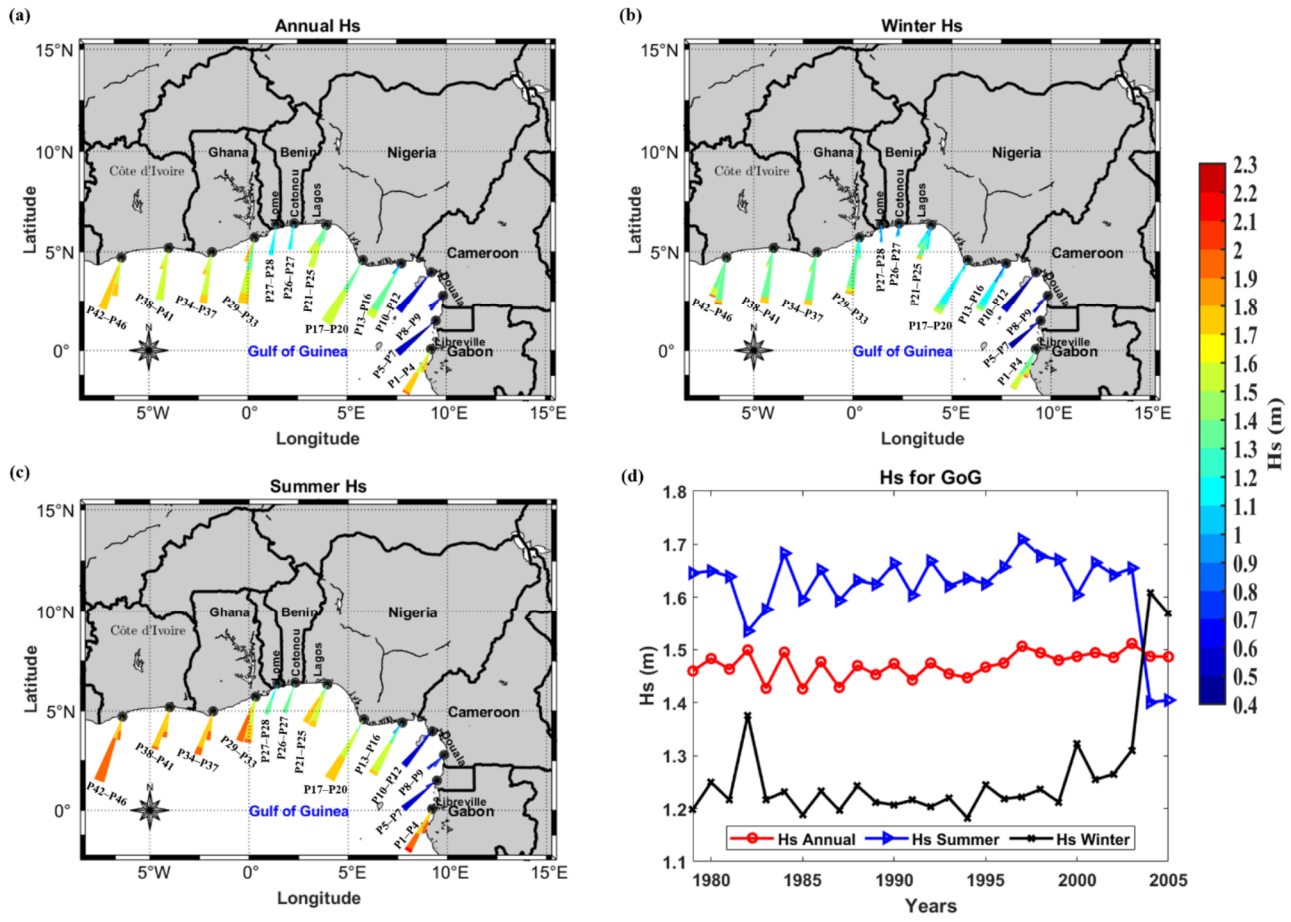

Figure 2. Wave roses showing direction-oriented spatial distribution of the average (**a**) extreme annual *Hs* (**b**) extreme winter *Hs* (**c**) extreme summer *Hs* and (**d**) timeseries of *Hs* between 1979–2005.

As presented in Table 2, the annual average of extreme *Hs*, as shown in Figure 2a, is estimated to be 1.47 m while the seasonal average for the extreme *Hs* during the dry (winter) season is 1.26 m (Figure 2b) and the wet (summer) season is 1.62 m (Figure 2c). These results confirm that higher extreme *Hs* are observed during the summer than in winter which can be explained from spatial distribution in Figure 2b–c where values as low as 0.4 m are seen further west in the winter unlike in the summer where values as high as 2.2 m was recorded in the upper northwest (Cote d'Ivoire) and lower southeast (Gabon).

Table 2. Average extreme *Hs* and its trends for the period 1979–2005.

Wave Climate	Annual	Winter	Summer
Extreme *Hs* (m)	1.47	1.26	1.62
Extreme *Hs* trend (m per year)	1.4×10^{-3}	6.3×10^{-3}	-2.1×10^{-3}

The spatial distribution of the *Hs* trend shown in Figure 3 shows that the *Hs* in the GoG has been experiencing an increase on an annual basis though this is not uniform throughout the year. The trend in the summer shows a decrease as high as -2.8×10^{-3} while a generally increasing trend up to 8.3×10^{-3} is seen in the winter. The annual trend analysis for the period 1979–2005 showed that *Hs* increased with the highest rates in the winter as can be observed in Table 2. As summarized in Table 2, the average annual increase is 1.4×10^{-3} m per year while the winter rate is 6.3×10^{-3} m per year, but the

Hs experienced a decreasing trend at the rate of 2.1 $\times$ 10^{-3} m per year in the summer. The Mann–Kendall test carried out to show the significance of these trends is denoted by the asterisk marker in Figure 3. It shows that for the annual and winter trends, most locations in the GoG have been experiencing a significant increase in *Hs*. Contrary to this, the decrease estimated for the summer season shows no statistical significance anywhere in the GoG. Worthy of note is the fact that regions with the highest values of extreme *Hs* as shown in Figure 2 also coincide with where higher increasing trends are being experienced in the GoG. For example, the locations lying between Cote d'Ivoire and the western part of Nigeria (P14–P46) generally show trends higher than 6.0 $\times$ 10^{-3} in the winter. This weakened in the low *Hs* region seen from Niger Delta in Nigeria through Cameroon to Equatorial Guinea (P5–P13) and returned to higher trend values in Gabon (P1–P4) where extreme *Hs* are again high.

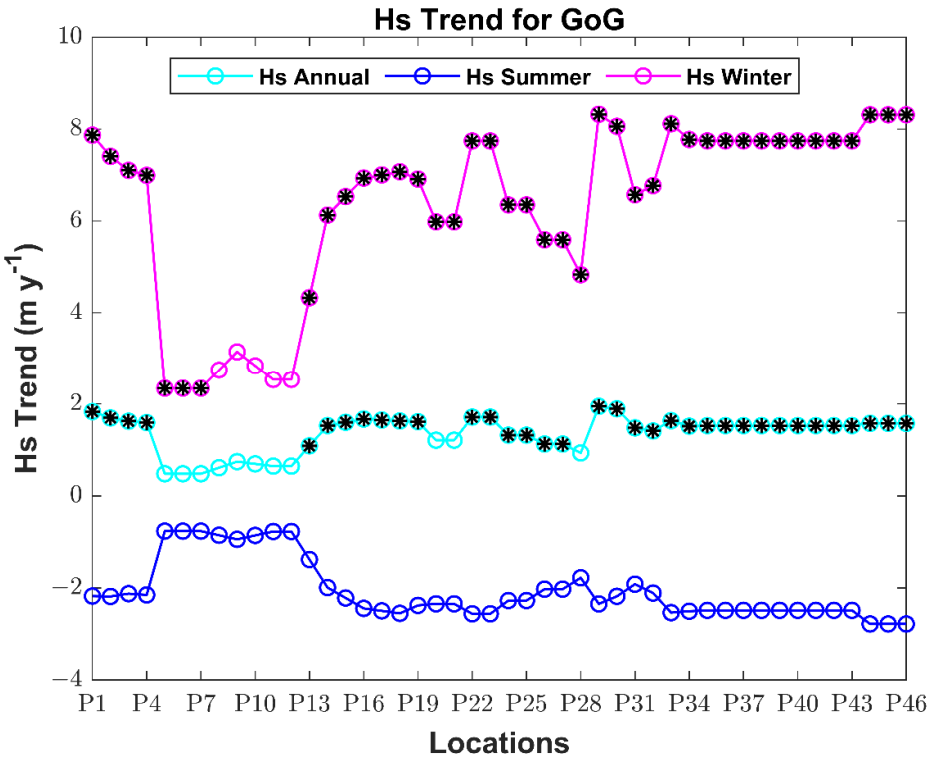

Figure 3. Line plot of the annual, winter and summer trends of *Hs* with asterisk showing locations with significant trend. Asterisk (*) represents significant *Hs* trend.

From Figure 4a–c, it can be observed that the mean wave period shows little variations both spatially and temporally in the GoG. Except for noticeable variation around Eastern Cameroon through Equatorial Guinea, the average *Tm* is uniform around the year. The annual average for the extreme *Tm* is estimated to be 10.65 s while the seasonal values are 10.37 s and 10.86 s for winter and summer, respectively (Table 3).

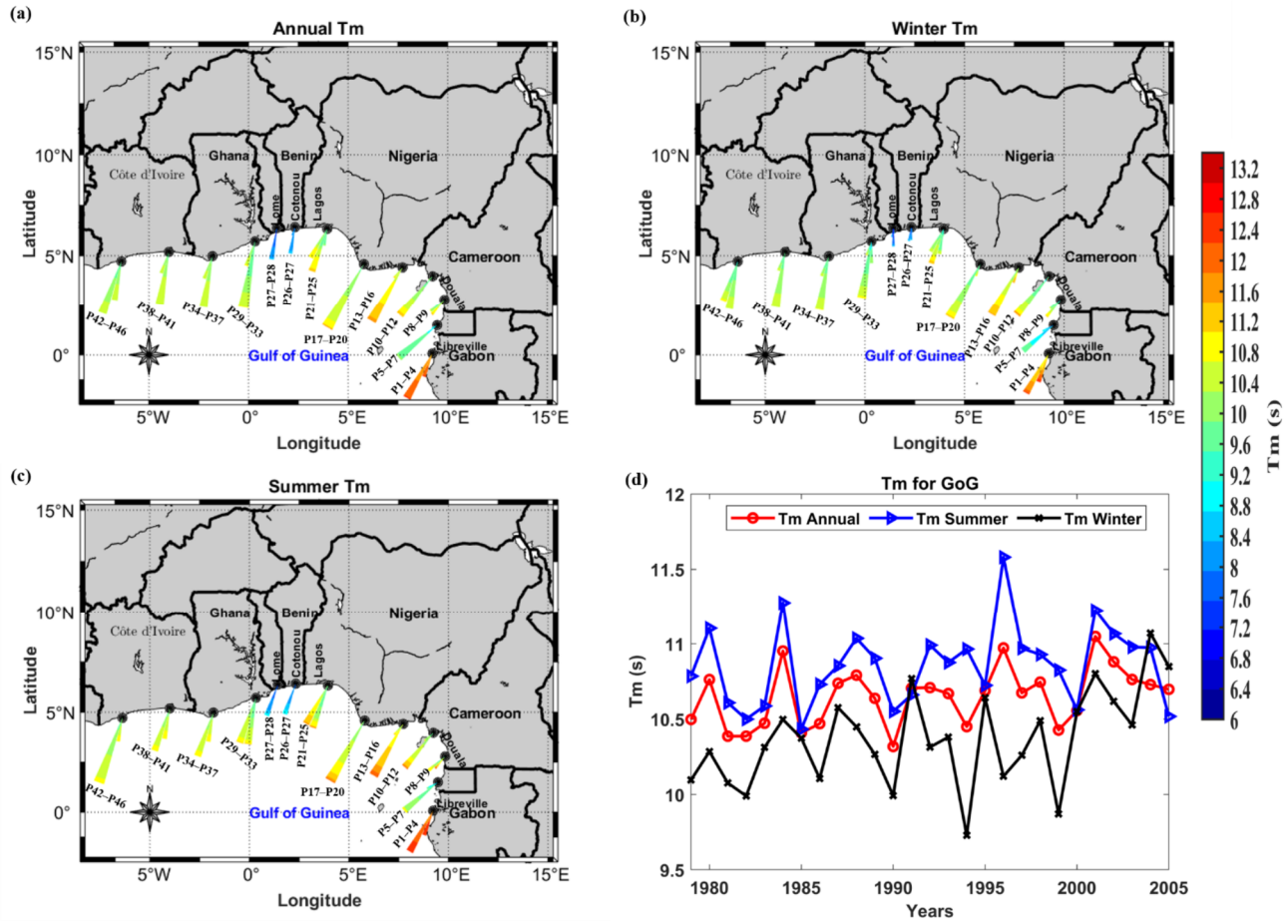

Figure 4. Wave roses showing direction-oriented spatial distribution of average (**a**) extreme annual *Tm* (**b**) extreme winter *Tm* (**c**) extreme summer *Tm* (**d**) timeseries of *Tm* between 1979–2005.

Table 3. Average extreme *Tm* and its trends between 1979–2005.

Wave Climate	Annual	Winter	Summer
Extreme *Tm* (s)	10.65	10.37	10.86
Extreme *Tm* trend (s per year)	9.7×10^{-3}	18.7×10^{-3}	7.3×10^{-3}

The average *Tm* trend on annual, winter and summer bases are 9.7×10^{-3}, 18.7×10^{-3} and 7.3×10^{-3} s per year, respectively. This was confirmed by visually observing the winter trend values which are higher than others though they all follow similar spatial variability (Figure 5). The Mann–Kendal test of trend significance showed that the *Tm* trend is insignificant in most parts of the GoG though significant in the center of the GoG between the Benin Republic and Eastern Ghana in the winter and on annual basis. This region of a significant increase in *Tm* extends a little southeastward to P18 on the Nigerian coast during the winter though this is not a region-wide continuous significant trend as seen in the case of *Hs*. A noteworthy observation in Figure 5 is that the northwestern part of GoG between Cote d'Ivoire and the western coast of Ghana (P34–P46) shows very low rates of increase in *Tm* contrary to the other regions with a similar trend in *Hs* previously mentioned.

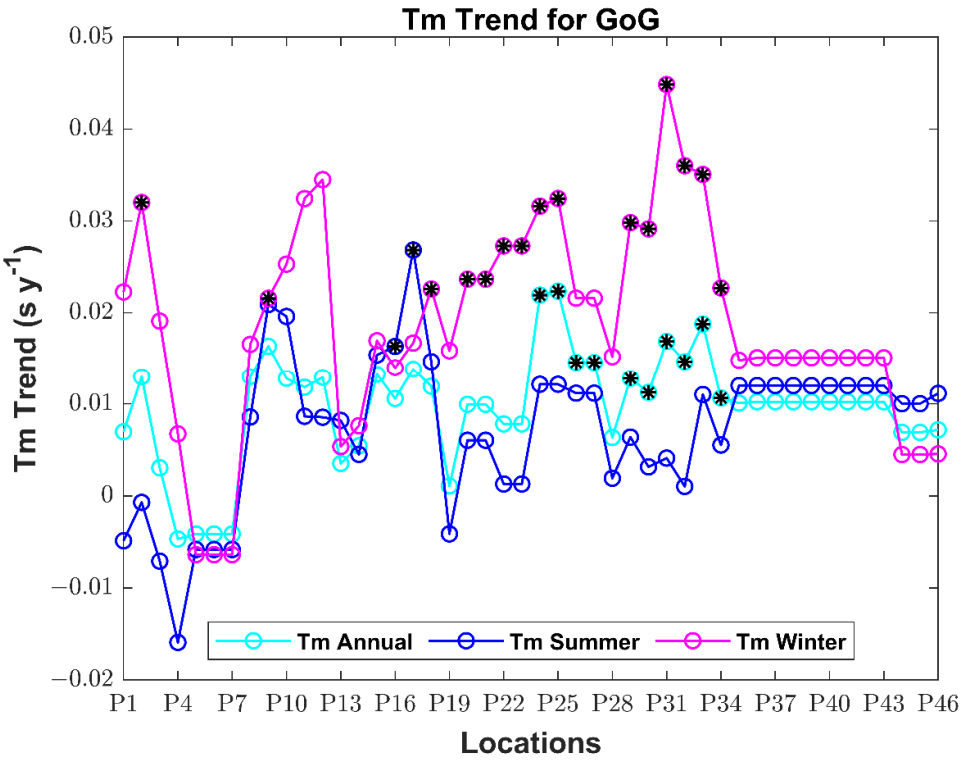

Figure 5. Line plot of the annual, winter, and summer trends of *Tm* with asterisk showing locations with a significant trend. Asterisk (*) represents significant *Tm* trend.

Similar to the predominantly S-SW wave direction reported for the GoG, the annual average of *Dm* estimated in this study, clockwise from north, is 204.39° while the winter and summer mean wave directions are 201.89° and 206.27° (S-SW). The waves in the GoG seemed to be more oriented to the north with more southerly origin in the western part of the GoG, from Cote d'Ivoire to the Benin Republic, with values generally ranging from 180–199°. A shift to more southwesterly moving in the northeast direction towards the coast is seen from Nigeria which gets more southwesterly towards Equatorial Guinea (Figure 6a–c). The trend analysis showed that, on average, the wave direction in the GoG between 1979–2005 experienced an anticlockwise shift, i.e., it dominantly originated from the south (northward direction towards the coast) at a decreasing rate of 29.2×10^{-3} degrees per year while decreasing rates of 12.6×10^{-3} and 6.7×10^{-3} degrees per year are estimated for winter and summer, respectively (Table 4). The Mann–Kendal test did not reveal statistical significance in these trends though locations P10, P15, and P29 showed some statistical significance (Figure 7).

Table 4. Average extreme *Dm* and its trends between 1979–2005.

Wave Climate	Annual	Winter	Summer
Extreme *Dm* (°)	204.39	201.89	206.27
Extreme *Dm* trend (° per year)	-29.2×10^{-3}	-12.6×10^{-3}	-6.7×10^{-3}

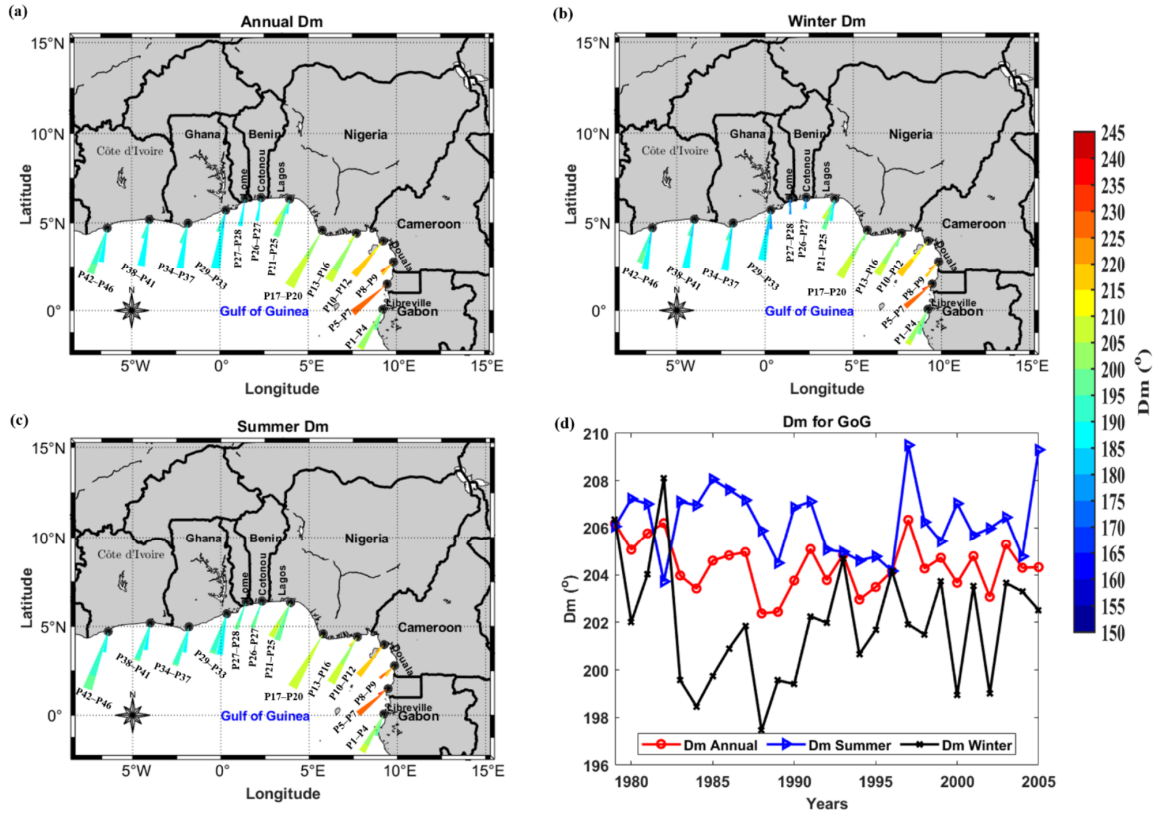

Figure 6. Wave roses showing direction-oriented spatial distribution of average (**a**) extreme annual *Dm* (**b**) extreme winter *Dm* (**c**) extreme summer *Dm* (**d**) timeseries of *Dm* between 1979–2005.

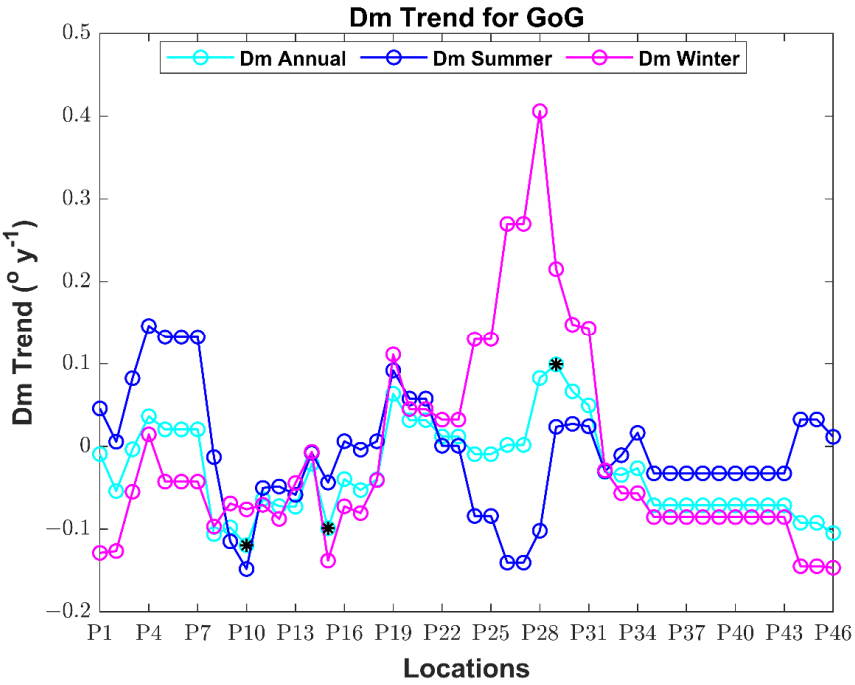

Figure 7. Line plot of the annual, winter, and summer trends of *Dm* with asterisk showing locations with a significant trend. Asterisk (*) represents significant *Dm* trend.

The spatial variation of the trend values showed a high seasonal fluctuation in the wave direction in the coastal areas of the Benin Republic and Togo between P24–P28. This is evident in values recorded for the summer and winter trends in Figure 7 where

Dm in the summer and winter show opposite signs. The summer *Dm* trends decrease at rates ranging from 8.4×10^{-2}–14×10^{-2} degrees per year while the reverse is the case during the winter with *Dm* increasing at rates between 13×10^{-2}–41×10^{-2} degree per year. Nevertheless, the annual average in this region is shifting into a more southwesterly orientation (and moving in a northeast direction towards the coast. The summer showed a high rate of clockwise (westerly) shift while the winter showed more waves becoming increasingly southerly (anticlockwise shift). Another region with different signs of *Dm* is seen in Gabon (P44–P46) where the *Dm* is reducing into becoming more southerly in the winter at rates ranging from 14×10^{-2} degree per year. This changed to increase with a more southwesterly wave in the summer with values up to 3.3×10^{-2} degree per year. These inter-seasonal variabilities will impact the sediment drift in this coastal area and need to be monitored for erosion and accretion hotspots. Apart from the southernmost part of the GoG around Gabon, most points in the northwestern part showed a decrease in wave direction (clockwise shift) throughout the year. This majority decrease contributed to the negative average value reported in Table 4 though a closer observation of the values from one location to another showed some spatial variations. This spatial variation in wave direction trend can be observed in places such as P1–P7 and P18–P23 in addition to the other two regions around the Benin Republic and Gabon. This observation emphasizes the need for a location-based analysis of wave climate in these regions rather than extrapolating the regional wave condition in the GoG for every country in the region.

The need for this aforementioned location-based further analysis of wave conditions is readily explainable when one compares the trend values for some locations with the average regional values presented in Table 4. For example, the regional average *Dm* trend for the whole GoG showed a decrease in the wave direction. This means the wave direction is experiencing an anticlockwise shift from a southwesterly orientation into a more southerly orientation. However, this is not totally a representation of the change occurring between P4–P7 where positive trends are seen for the annual average and summer. This region thereby shows a clockwise shift in wave direction from a southwesterly into a more southwesterly which is contrary to the anticlockwise shift estimated for the whole GoG. Another location of deviation from the regional average lies between P19–P31 which has the Volta Delta to the west and Niger Delta to the east. This location showed a majorly positive trend for the seasonal and annual averages with very few exceptions which are very low negative values. In the westernmost part of Cote d'Ivoire between P44–P46, another local deviation from the regional mean was also observed. These observed deviations mean that the local fluctuation at a location is not necessarily deducible from the regional average. Hence, the need for local monitoring of wave conditions in these aforementioned locations of deviation from the regional average is very important to have a clearer understanding of the variations in the wave climate in these areas. This local deviation can be linked to the contribution to the wave condition from local winds creating wind seas which influence the swell in the location. This would have been clearer if local observations data are available for analysis This is owing to the fact that swell waves represent more of the variabilities in the storm conditions where they are generated. These swell waves, even though they are dominant, are combined with locally generated wind waves. These combined waves, which were modeled by the data source in this study, determine the average wave climate in a location which means the strength and orientation of local winds contribute to the overall wave direction.

4.2. Future Change in Extreme Wave Climate

The assessment of the future wave climate for the mid-century (2026–2045) and end-century (2081–2100) was done under RCP 4.5 and RCP 8.5. The changes between the past and the future were also assessed as the difference between the average of the historical and future wave climate. The results are presented for *Hs*, *Tm*, and *Dm* in this subsection.

Figure 8a–c show that the spatial distribution of extreme *Hs* in the GoG for the periods 2026–2045 and 2080–2100 seems to have a similar trend for both RCP 4.5 and RCP 8.5. The

usual spatial west-to-east decrease in *Hs* known in the GoG and shown in Figure 2 for the historical time slice continues for all time slices and RCP scenarios. The minimum *Hs* zone between Cameroon and Equatorial Guinea can also be observed at the locations between P5-P13 in Figure 8a–c. The transition into higher values occurs southeastward in Gabon (P1–P4) and a slight reduction in the Volta Delta (P30–P31). The overlap of the lines of the different time slices and climate change scenario shows that the difference is not much. The average values for the different time slices and RCP scenarios in Table 5 also confirm this closeness. This closeness was also confirmed by the results of the ANOVA and Tukey–Kramer tests graphically shown by the boxplots in Figure 9 and summarized in Table 6. The high *p*-values (greater than 0.9) and low F-values show that the *Hs* for the various RCP scenarios for both mid and century time slices are not significantly different from one another. All these aforementioned closeness in values of extreme *Hs* have similar patterns around the year as seen on seasonal and annual plots (Figure 8a–c). The statistical tests also confirmed this same pattern for annual, winter, and summer *Hs* with the overlap of the boxplots for all these periods shown in Figure 9.

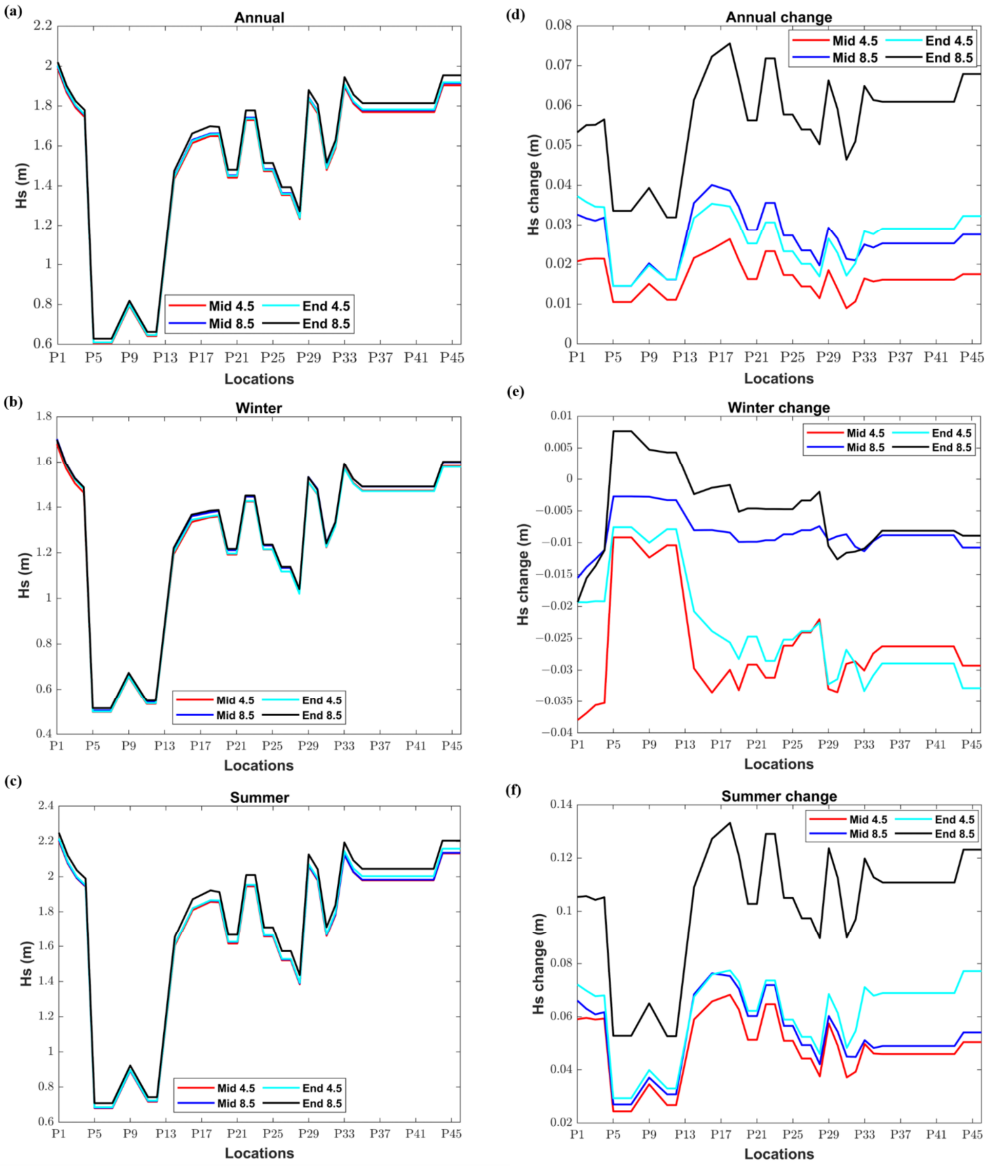

Figure 8. Line plots of the extreme *Hs* presented as averages for (**a**) annual (**b**) winter, and (**c**) summer. Average change in extreme *Hs* relative to the past for all future time slices and RCP scenarios for (**d**) annual (**e**) winter, and (**f**) summer.

Table 5. Mid and end-century average extreme *Hs* and change relative to the past.

Time Slice	RCP Scenario	Annual Average (m)	Annual Change (m)	Winter Average (m)	Winter Change (m)	Summer Average (m)	Summer Change (m)
Mid century (2026–2045)	RCP 4.5	1.49	0.017	1.24	−0.026	1.67	0.048
	RCP 8.5	1.50	0.027	1.25	−0.0083	1.67	0.052
End century (2081–2100)	RCP 4.5	1.50	0.026	1.24	−0.023	1.68	0.061
	RCP 8.5	1.53	0.056	1.26	−0.0049	1.72	0.10

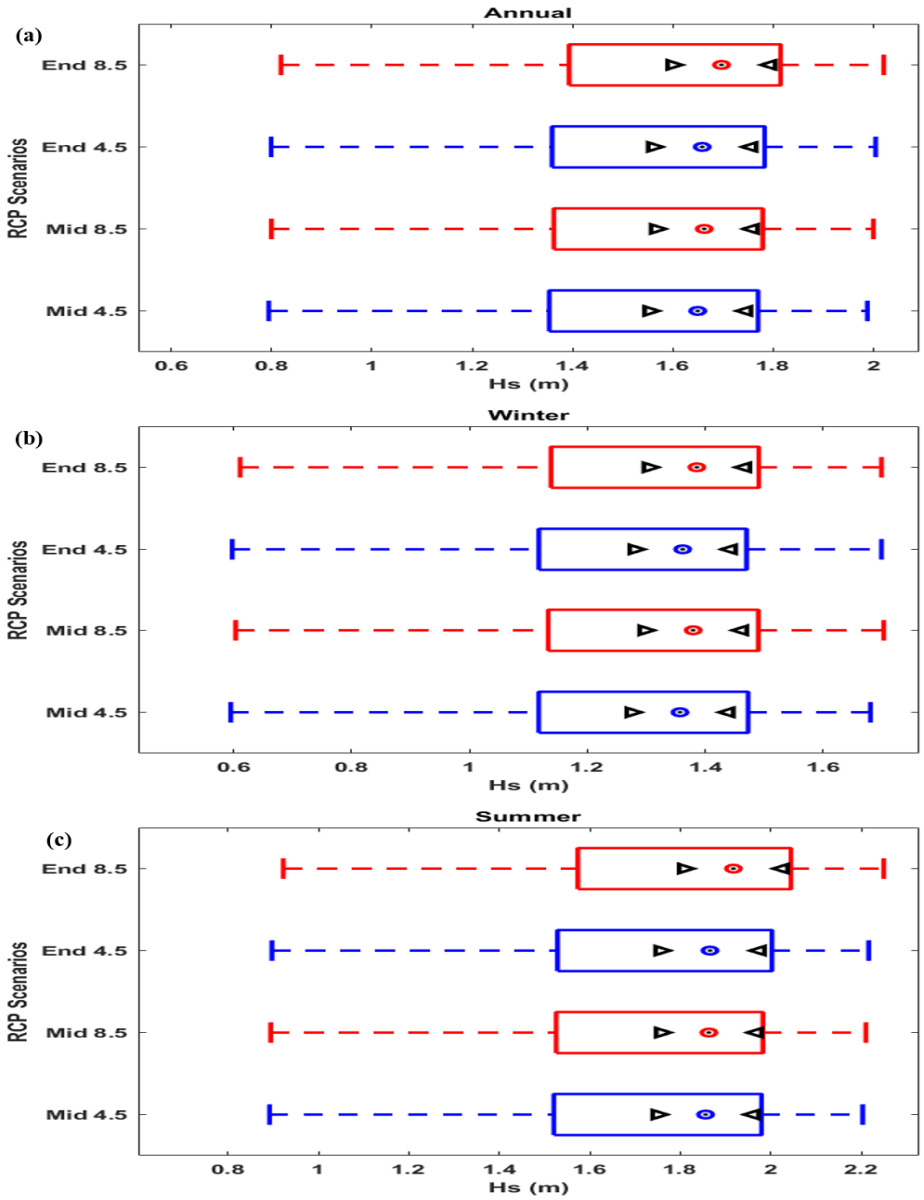

Figure 9. Boxplots showing the overlaps between *Hs* means for all future RCP scenarios with blue and red boxplots representing the RCP 4.5 and RCP 8.5, respectively for (**a**) annual (**b**) winter (**c**) summer.

Table 6. Summary of the output ANOVA and Tukey–Kramer tests for future extreme *Hs*.

Period	F-Value	*p*-Value
Annual	0.0729	0.9744
Winter	0.0392	0.9896
Summer	0.1191	0.9488

For the mid-century (2026–2045), the average annual *Hs* as presented in Table 5 shows higher values under RCP 8.5 than RCP 4.5. In the winter, the average estimated is also lower than the summer averages still maintaining higher values under RCP 8.5 than RCP 4.5. From the results presented in Figure 8a, by the end of the century (2081–2100), the annual average is projected to follow the similar spatial distribution seen in the mid-century for the RCP scenarios (4.5 and 8.5). The overlap in the lines in Figure 8b–c confirmed that seasonally (winter and summer), there will not be many variations as well. These results show that the *Hs* at the end of the century by 2100 is expected to be higher than in the past and mid-century for all the seasons. Additionally, the projections under RCP 8.5 show higher waves on the coast of the GoG for both mid and end-century simulations.

Relative to the historical time slice (1979–2005), the change in extreme *Hs* for all the future time slices is shown in Figure 8d–f. The average change between the past and mid-century are 0.017 and 0.027 m for the RCP 4.5 and RCP 8.5, respectively. Relative to the end of the century, the average changes are projected to be 0.026 and 0.056 m, respectively (Table 5). A higher rate of increase is projected under RCP 8.5 than RCP 4.5 for the annual average.

During the winter, the changes in extreme *Hs* from past to mid-century are expected to decrease with more decrease expected under the RCP 4.5 climate conditions. This means a higher difference between the past winter *Hs* conditions and the winter *Hs* simulated under RCP 4.5. This is expected to continue till the end of the century. When the average *Hs* change values for the mid and end century are compared for both RCP 4.5 and RCP 8.5, the results show that the winter *Hs* decrease will slow down by the end of the century since the difference between past and mid-century is more negative than difference with the end-century. Characteristically, the summer results are similar to the annual average in that the increase in *Hs* by end of the century is higher than by mid-century with a change as high as 0.1 m projected by 2100.

In contrast to the *Hs* plots for both annual and summer averages (Figure 8d and 8e, respectively), the winter average change (Figure 8f) shows an almost inverted pattern to the others. One of the most noticeable contrasts is the higher *Hs* change seen around Cameroon to Equatorial Guinea (P5–P12) known for low waves. In these locations, the least negative *Hs* values are found and, in some cases, even positive, suggesting the least *Hs* change values in the winter in this region. This can be translated as, though a reduction in *Hs* is projected during the winter for the GoG in the future, the Cameroonian–Equatorial Guinea region might experience around the year increase in *Hs* as shown in Figure 8f by the line for the RCP 8.5 for the end-century time slice. However, this is not a high change compared to other parts of the GoG as seen in the locations around P5-P12 which are known for relatively low values for extreme *Hs* (Figure 8a–c).

Looking at Figure 10a–c, similar to the observation for *Hs*, the average of the extreme values of wave period for all the time slices (summarized in Table 7) follow similar trends with little differences. The spatial distribution of the *Tm* values is similar to the ones seen for *Hs* as the locations P1–P4 in the southernmost part of the GoG (Gabon) have the highest values, all greater than 12 s. This is followed by the region of mostly low *Hs* values, locations between Cameroon and Equatorial Guinea (P5–P12) also have decreasing *Tm*. The lowest values of *Tm* are found between the Benin Republic and Togo (P25–P27) with values below 9 s. Coincidentally, the areas of lower *Tm* coincide with the region projected to have the highest changes occurring in the future when Figure 10a–c (average future extreme *Tm*) are compared with the neighboring Figure 10d–f (change in future extreme

Tm relative to the past). Again, the most noticeable spatial fluctuations are seen between the southwestern and southeastern parts of Nigeria (P13–P24). The points from the Bight of Benin westward to Cote d'Ivoire (P33–P46) have relatively uniform *Tm* values. Similar to the case of *Hs*, the *Tm* for both future time slices (mid and end-century) for all the RCP scenarios were compared. The summary of the statistical test results in Table 8 and the overlaps of the boxplot in Figure 11 showed that the *Tm* has close values as well. This is easily verifiable in the line plot of averages for each location (P1–P46) in Figure 10.

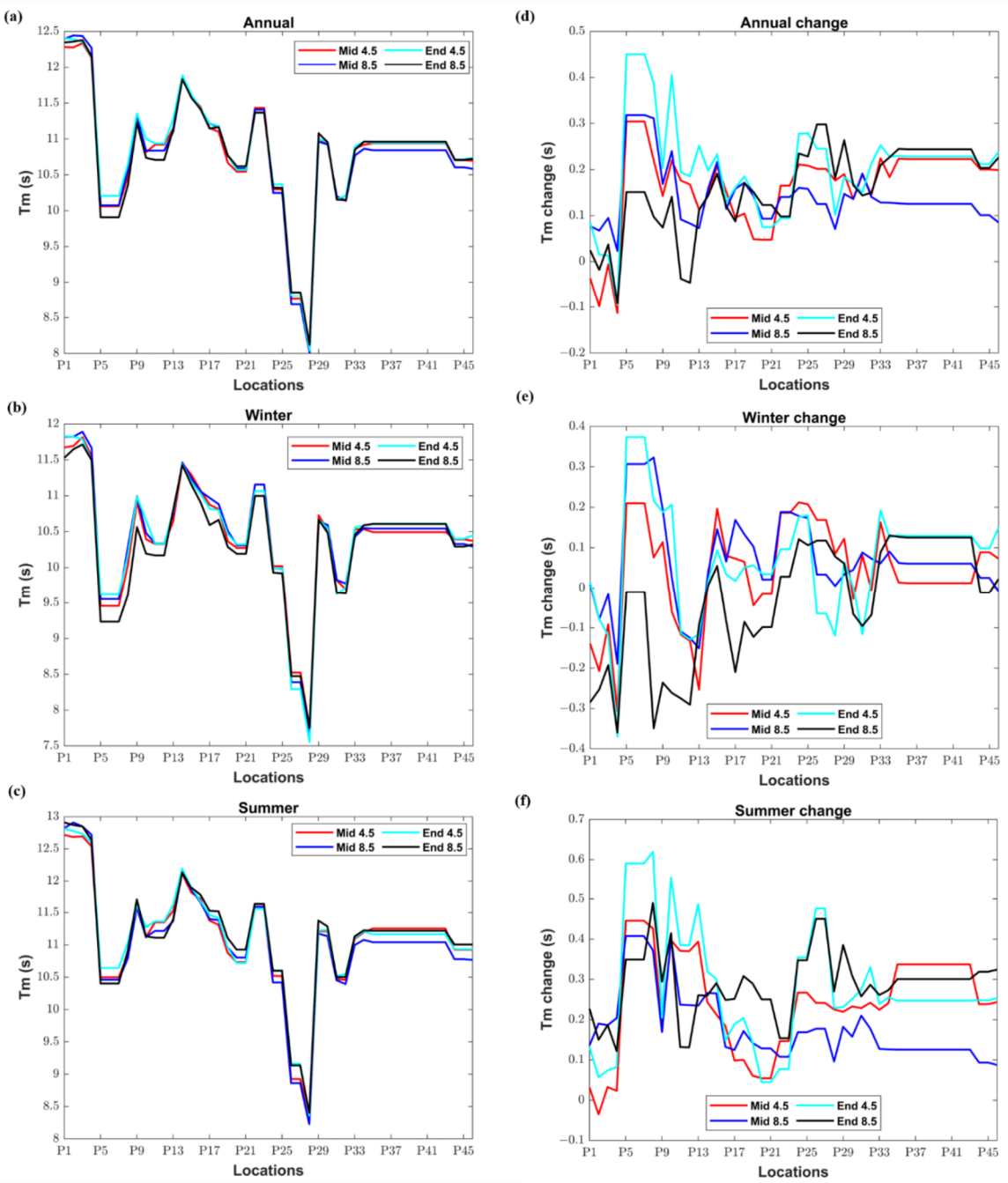

Figure 10. Line plots of the extreme *Tm* presented as averages for (**a**) annual (**b**) winter, and (**c**) summer and average change in extreme *Tm* relative to the past for all future time slices and RCP scenarios for (**d**) annual (**e**) winter, and (**f**) summer.

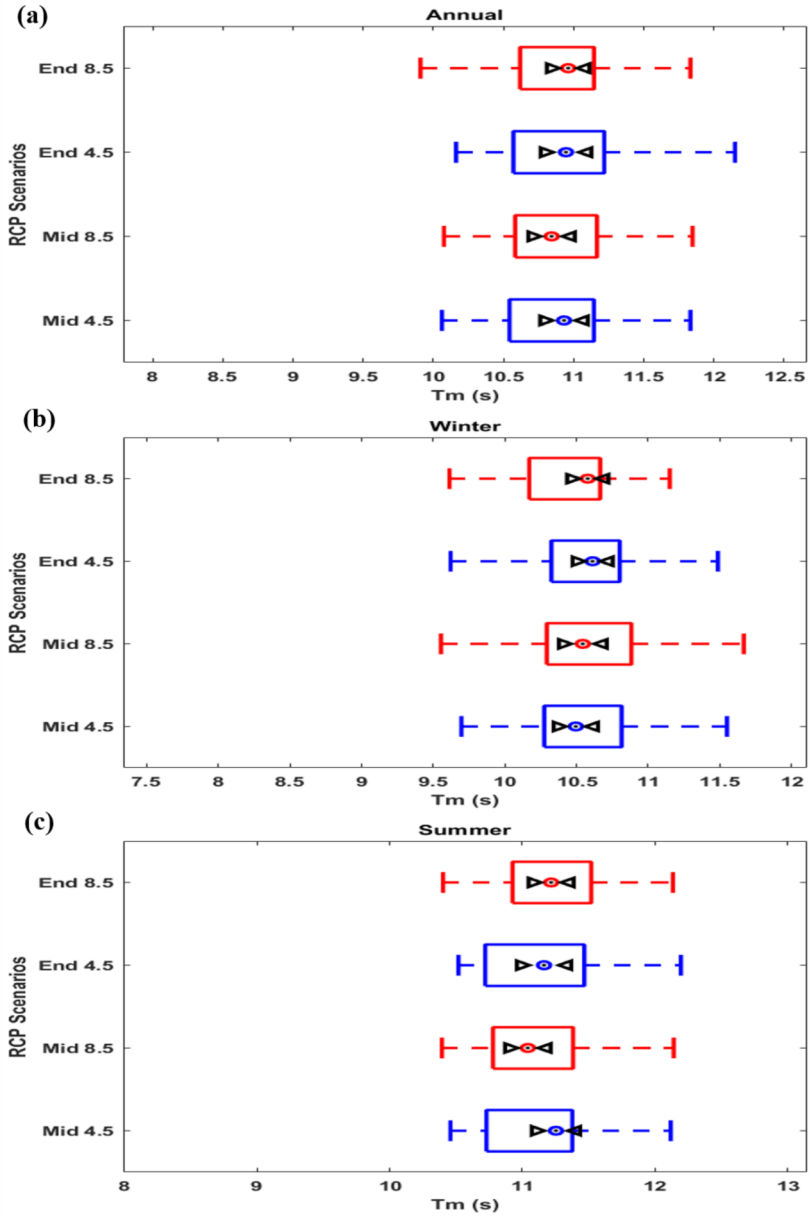

Figure 11. Boxplots showing the overlaps between *Tm* means for all future RCP scenarios with blue and red boxplots representing the RCP 4.5 and RCP 8.5, respectively for (**a**) annual (**b**) winter (**c**) summer.

Table 7. Mid and end-century average extreme *Tm* and change relative to the past.

Time Slice	RCP Scenario	Annual Average (s)	Annual Change (s)	Winter Average (s)	Winter Change (s)	Summer Average (s)	Summer Change (s)
Mid-century (2026–2045)	RCP 4.5	10.81	0.16	10.41	0.040	11.10	0.24
	RCP 8.5	10.79	0.14	10.44	0.071	11.04	0.18
End-century (2081–2100)	RCP 4.5	10.86	0.21	10.49	0.071	11.14	0.28
	RCP 8.5	10.81	0.16	10.34	−0.032	11.15	0.29

Table 8. Summary of the output ANOVA and Tukey–Kramer tests for future extreme *Tm*.

Period	F-Value	*p*-Value
Annual	0.0472	0.9863
Winter	0.1617	0.9220
Summer	0.1410	0.9353

The annual average *Tm* for mid-century (RCP 4.5 and RCP 8.5) and end-century (RCP 4.5 and RCP 8.5) are summarized in Table 7. A close observation of the values presented for the various time slices and climate change scenarios reveal that the projections under RCP 4.5 showed higher *Tm* values than RCP 8.5 for both mid and end-century on annual basis. This pattern is not consistent with either summer or winter analysis; although the summer for both RCP scenarios showed that the *Tm* increased by the end of the century similar to the annual values, unlike winter which showed decreasing *Tm* by the end of the century for RCP 8.5. Likewise, the changes in *Tm* relative to the past also follow similar annual and seasonal trends for all the time slices. Similar to the case with projected changes for *Hs*, the magnitude of the change between the historical time slice and the future wave period is relatively low. The highest change projected to happen for RCP 8.5 by the end of the century only amounts to less than a 3% increase. This seemingly insignificant change is important as it will contribute to shaping the wave action experienced in the coastal areas in the GoG, especially in conjunction with other indices of climate change such as increasing water levels.

Figure 12a–c reiterates the predominantly S-SW orientation of wave in the GoG with averages for mid-century and end-century for both RCP 4.5 and RCP 8.5 projected to be between 180°–235°. In the winter, an anticlockwise shift makes the direction more southerly oriented while a more southwesterly direction is projected for the summer (Table 9). The usual closeness of the values for the different time slices and RCP scenarios reported for both *Hs* and *Tm* is also observed for *Dm*. This similarity of Dm was tested for statistical difference and the results are presented in Table 10 and Figure 13. The overlapping boxplots as well as the F-values and *p*-values depict no significant difference. This means the *Dm* follows a similar spatial distribution with very close values regardless of the climate change scenario considered for the wave conditions in the GoG.

Table 9. Mid and end-century average extreme *Dm* and change relative to the past.

Time Slice	RCP Scenario	Annual Average (°)	Annual Change (°)	Winter Average (°)	Winter Change (°)	Summer Average (°)	Summer Change (°)
Mid-century (2026–2045)	RCP 4.5	204.88	0.48	202.20	0.31	206.74	0.47
	RCP 8.5	204.93	0.54	202.50	0.61	206.63	0.35
End-century (2081–2100)	RCP 4.5	205.09	0.69	202.81	0.92	206.75	0.48
	RCP 8.5	206.58	2.19	204.80	2.92	207.78	1.51

Table 10. Summary of the output ANOVA and Tukey–Kramer tests for future extreme *Dm*.

Period	F-Value	*p*-Value
Annual	0.2149	0.8860
Winter	0.3954	0.7564
Summer	0.1029	0.9583

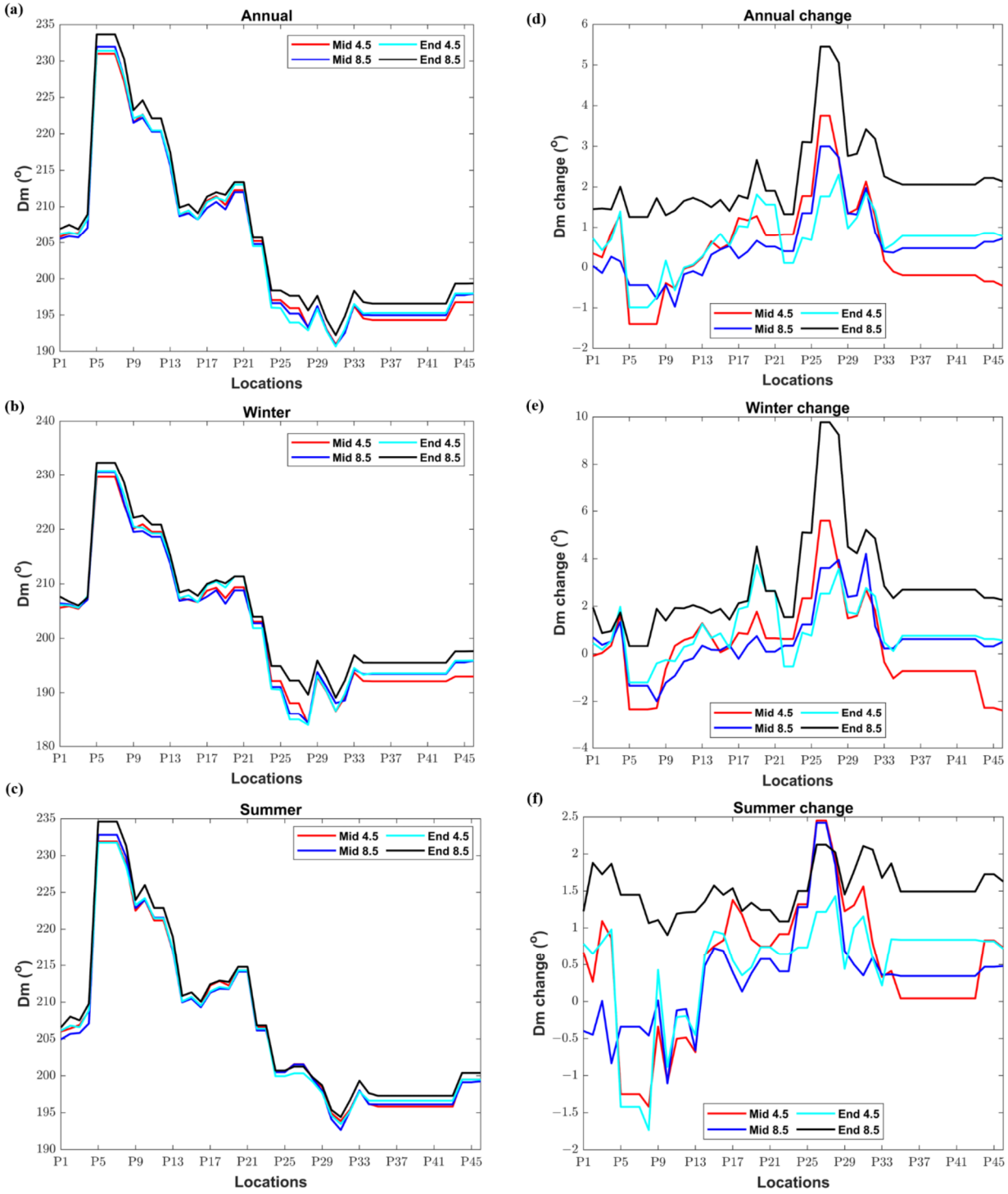

Figure 12. Line plots of the extreme *Dm* presented as averages for (**a**) annual (**b**) winter, and (**c**) summer and average change in extreme *Dm* relative to the past for all future time slices and RCP scenarios for (**d**) annual (**e**) winter, and (**f**) summer.

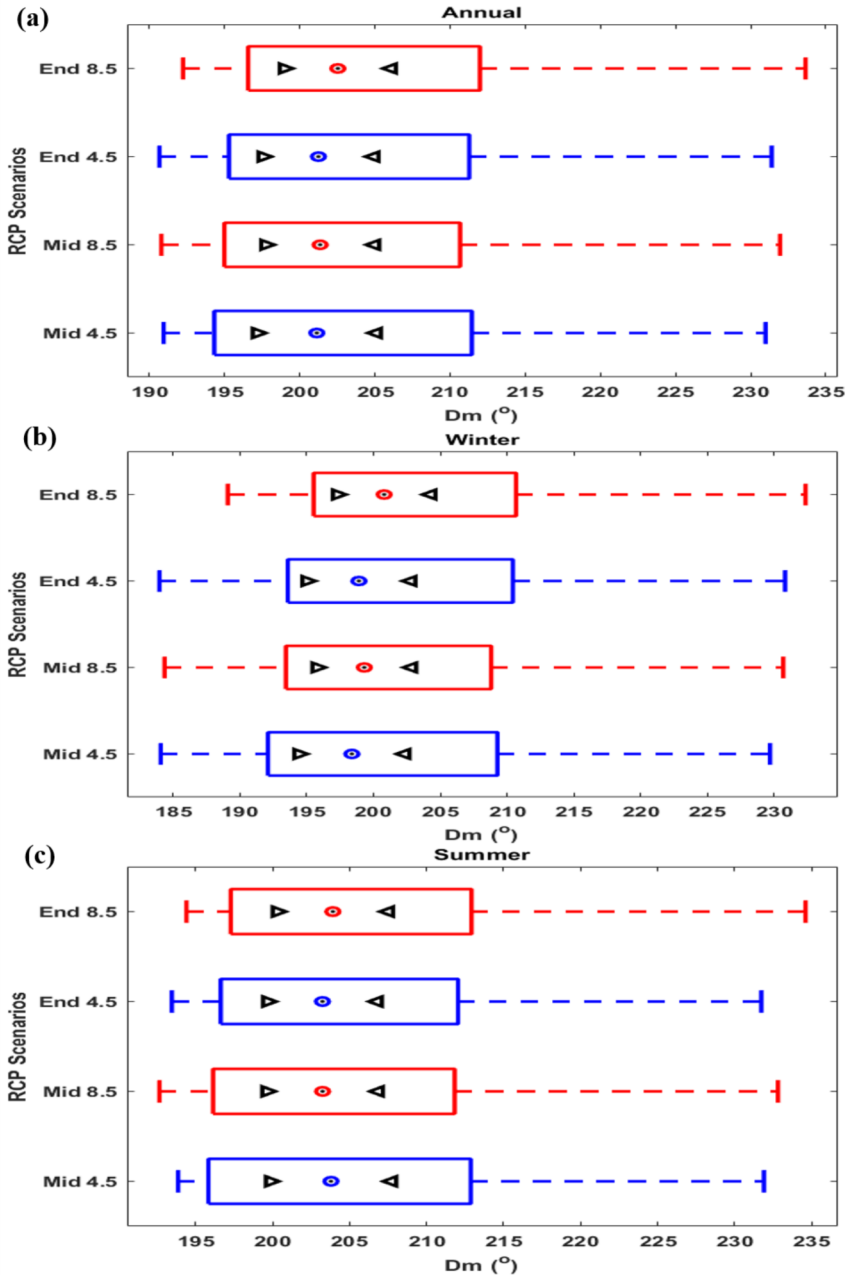

Figure 13. Boxplots showing the overlaps between *Hs* means for all future RCP scenarios with blue and red boxplots representing the RCP 4.5 and RCP 8.5, respectively for (**a**) annual (**b**) winter (**c**) summer.

A closer observation of the wave direction presented in Figure 12a–c shows different bins of wave direction which correlates with the varying orientation of the coastline in the GoG. This is merely a visual observation that does not necessarily translate to the influence of coastline orientation on the simulated wave climate because the native spatial resolution of the model data ($1^\circ \times 1^\circ$) does not support such a direct deduction. Starting from the northwesternmost part of GoG, Cape Palmas in Liberia (P46) to San Pedro in Cote d'Ivoire (P44), a brief uniform wave direction is seen around the eastward slope of the cape. Eastward of this region to Takoradi in Ghana (P35) has a similar wave direction also. The next section of the coast has rapidly varying wave direction and stretches between Cape Coast to the Volta Delta before Togo (P34–P30). A closer look at the features in this region of rapidly varying *Dm* reveals several embayed beaches with differing *Dm* on the leeward and windward sides. This again is a mere visual observation of the nearby features

and not necessarily causation of the spatial variation in *Dm* values. Another similar wave direction is found between Togo and Benin Republic (P29–P25) while the next one is the western coast of Nigeria followed by the Niger Delta, then the eastern coast of Nigeria. The ones in the south are the Cameroon–Equatorial Guinea stretch followed by the Gabon southernmost uniform coastline. A summary of the winter and summer maximum values of *Dm* in these uniform wave direction locations is presented in Table 11.

Table 11. Average extreme *Dm* (winter–summer) for uniform locations in the GoG.

Time Slice	Past (1979–2005)	Mid-Century (2026–2045)		End Century (2081–2100)	
RCP Scenario		**RCP 4.5 (°)**	**RCP 8.5 (°)**	**RCP 4.5 (°)**	**RCP 8.5 (°)**
Cape Palmas–San Pedro (P44–P46)	195.3–198.8	193.0–199.5	195.6–199.2	195.9–199.5	197.6–200.4
San Pedro to Takoradi (P35–P43)	192.8–195.8	192.1–195.8	193.4–196.1	193.6–196.6	195.5–197.3
Togo–Benin (P25–P29)	180.4–199.2	192.9–201.6	193.8–201.5	193.2–200.4	195.9–201.3
Western Nigeria (P18–P21)	205.6–213.6	207.3–212.9	208.8–214.1	211.4–214.3	211.3–214.8
Eastern Nigeria (P13–P17)	206.3–217−7	214.6–217.0	213.7–217.1	214.6–217.3	215.3–218.9
Cameroon–E. Guinea (P5–P9)	232.0–233.2	229.7–231.9	230.7–232.8	230.8–231.7	232.4–234.6
Gabon (P1–P4)	205.1–207.9	207.4–208.8	207.0–207.1	207.7–208.9	207.7–209.8

The difference between the past and future wave directions showed a general shift to a more southwesterly orientation since all the values show increased wave directions. This increase in wave direction is contrary to the decrease seen in the trend analysis performed on the past wave direction previously presented in Figure 7. Note that the Mann–Kendall test performed to test the significance of the *Dm* trend in Figure 7 did not show any significance for the trend performed for the past wave direction. This confirms the possible shift in wave direction from the current situation as seen in the past anticlockwise shift to a clockwise shift by the end of the century. The highest changes in wave direction are expected between the Benin Republic and Togo (P25-P29). In agreement with previous projections by previous global studies for the change in *Dm* by the end of the century, a clockwise rotation up to 2° should be expected along the West African coast as shown in Table 9. This translates to a change in *Dm* slightly above 1% of the past wave direction.

5. Discussion

5.1. Past Extreme Wave Climate and Trends

The result presented for extreme *Hs* in this study is consistent with the findings of previous studies that investigated past wave climate in the GoG. Firstly, the west-to-east decrease in *Hs* reported by [22,37] in the GoG corresponded with the results of the present study. As expected, the annual average of extreme *Hs* for the GoG found here is higher than the *Hs* of 1.36 m estimated for the Bight of Benin for the period 1979–2012 by [45]. The average annual maximum wave period estimated in this study is 10.65 s which when compared to the 9.6 s estimated for the annual average peak wave period by [45] is understandably lower. This value reported by [45] is lower than the value found in this study because the wave climate assessed in this study is extremely unlike the average wave climate used by [45]. The annual average wave direction value of 204.39° estimated here confirmed the wave direction has generally S–SW incidence as reported by [45]. A slight seasonal variation is observed with higher values in the summer compared to the winter suggesting more SW orientation in the summer. The results presented by [37] for the 5 days study of the wave condition on the Cote d'Ivoire coast also confirmed values as high as 2.0 m on the Ivorian coast. [46] also reported values generally higher than 1.0 m for the Ivorian coast similar to the values ranging between 1.4–2.0 m seen between P38–P46, in the present study. The study by [46] in the Bight of Benin which is the coastal waters of the western part of the GoG also reported lower values of *Hs* during the boreal winter. On a regional basis, the results are within a reasonable range of findings from previous studies such as [22,37,45,57]. In the investigation of wave energy in the mid-Atlantic, [58]

confirmed that the values of *Hs* generally decrease from the west–east *Hs*, less than 1.2 m were reported for the southeastern mid-Atlantic where the GoG is located. The reported values and spatial trend of *Tm* are also similar though lower, as expected than the extreme *Tm* found in the present study. This is because the average wave condition was presented by [58] unlike the 99th percentile used in this study.

In the study assessing the impacts of wave dynamics on the coast of Ghana by [59], an average value of 1.39 m was reported as the mean wave height for the Ghana coast which, as expected, is less than the average values of 1.4–1.8 m observed around the same area (P29–P37). Additionally, the findings of [59] confirmed that higher waves are observed in August (summer). The peak wave period value of 10.91 s, as reported by [59], falls within 9.70–10.99 s found at this section of the GoG. The annual maxima *Hs* for the Keta–Volta delta coastal area of Ghana, as reported by [60], ranged between 2.5 and −3 m. [61] confirmed that 75% of the significant wave heights in the nearshore of the Ghana coast lie between 1 and 2 m. This agrees with the values found in the present study for both annual and seasonal averages since the lowest and highest values of approximately 1.2 and 2.0 m were found in the winter and summer, respectively. Additionally confirmed in this study is the sudden decrease in wave height around the Volta–Keta axis which returned to higher values from the Togo–Benin coast. This is seen in the results presented by [46] which also agrees with the reported different directions of wave in this part of the Ghanaian coast. This different orientation of waves in this region is obvious in the wave roses presented for the eastern coast of Ghana where lower waves with relatively different directions can be seen. This unique behavior of waves is reportedly due to the refraction they encounter as a result of the shallowness of the delta thereby preventing them from coming to the coast undisturbed. This deduction is strengthened by the fact that most of the points propagated to the coast for the analysis in this study all fall within the continental shelf of the locations being considered. As shown in Figure 14, some of the projected points off the coast of Ghana are less than 50 km to the coast in a region with a continental shelf as wide as 85 km with a shallow depth of lesser than 200 m as seen in Figure 1. For example, the data points propagated to the coastal locations in Cotonou, Lagos, and the cape of the Niger Delta are less than 10 km from the coast. This suggests that despite the model's native spatial grid of $1^\circ \times 1^\circ$, it still has points sufficiently close to the coast for coastal influence on the wave climate. This encounter, as expected, reduces energy by interacting with the seafloor thereby producing lower waves. This aforementioned relatively lower wave was linked by [60] to the effectiveness of the Volta–Keta axis in providing port service before the commencement of the Tema port (Figure 14b) in 1962. This was also noted in a study by [57] despite relying on data from ERA-Interim which has a similar native spatial grid as the COWCLIP data used in this study.

The low average and trend of *Hs* reported for the Cameroonian coast are also consistent, to an extent, with findings in studies by [62,63] where they reported maximum and average *Hs* of 0.7 and 0.27 m, respectively. However, [62] reported *Hs* trends of −0.001 m per year for the Cameroonian coast which agrees with the summer general decreasing trend of wave height in the GoG region including the Cameroonian coast. However, the values found for the Cameroonian coast in this study are an order of magnitude less than those in the other parts of the GoG. Additionally, this trend is not the same for both winter and summer though on an annual average, the Cameroonian coast has been experiencing an increase ranging from 0.00048–0.00074 m per year. The peak wave period of 12.29 s reported by [63] is slightly higher than the estimated extreme wave period that ranged from 10.44–11.41 s for locations between P9–P13. This disparity is most likely due to the short spatial and temporal coverage of their study, unlike the county-wide spatial coverage and long temporal coverage of the presented study that has averaged out such high values.

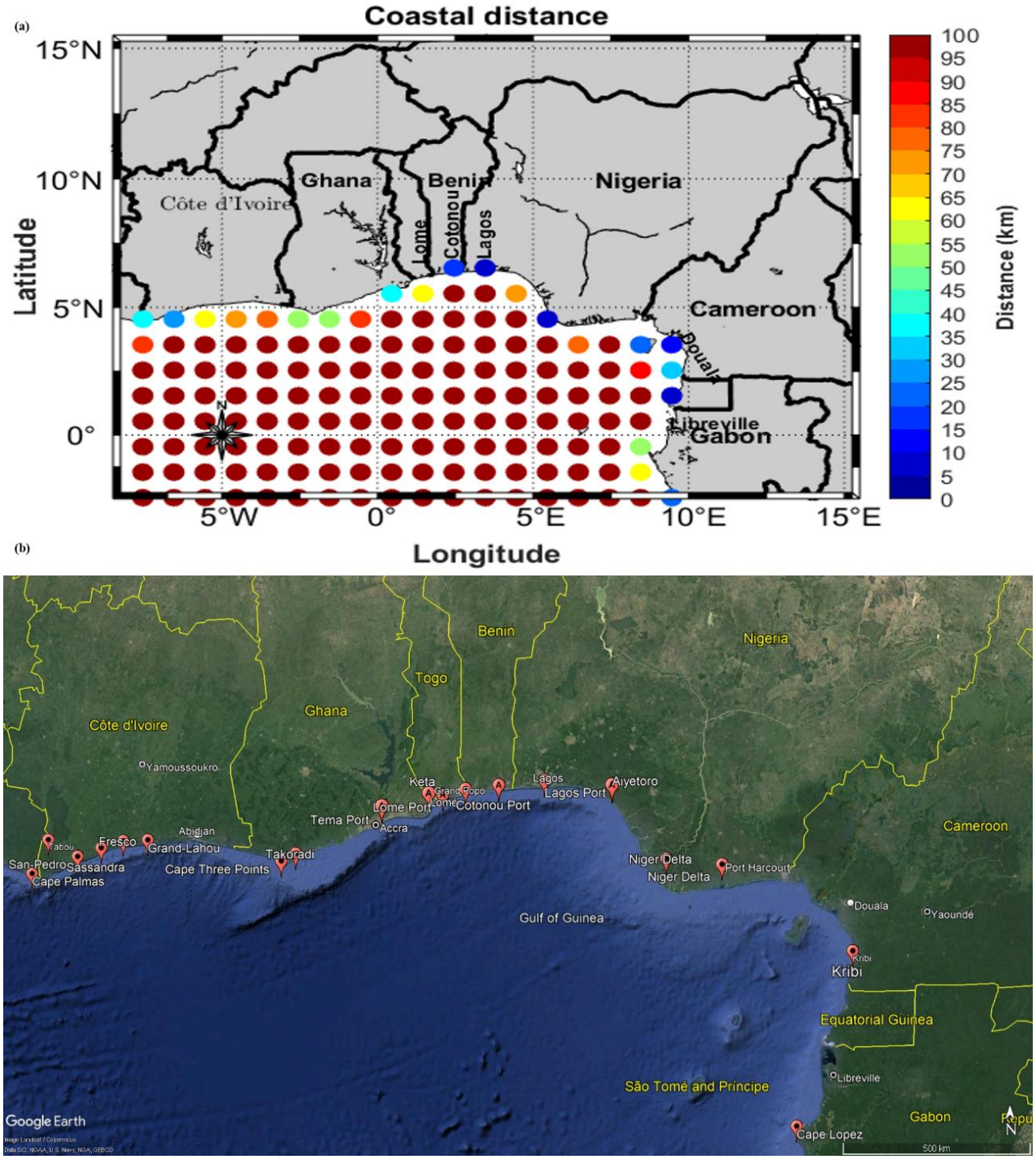

Figure 14. (**a**) Distance of each grid point to the nearest coastline in the GoG. (**b**) Map oof the GoG with some notable coastal structures on the continental shelf (light blue areas close to the coast).

In the study of the extreme *Hs* climate in the GoG, [22] estimated the annual trend of *Hs* between 1980–2016 to be 1.4×10^{-3} which is the same value found here. Similarly, the winter trend was estimated as an increase of 1.0×10^{-3} m per year though contrary to the slight decrease close to the coast found in this study, an increase was estimated by [22]. The disparity in results can be ascribed to the fact that this study chose specific points on the coast whereas [22] used the whole data points in a $0.1^\circ \times 0.1^\circ$ spatial resolution data covering the entire GoG including areas off the coast. Another point worthy of note is that the Mann–Kendal test performed to check the significance of these *Hs* trends presented in

Figure 3 showed that the rate of change is significant for almost all selected points in the GoG on annual basis. However, on a seasonal basis, only the *Hs* trend in winter showed a similar significant trend whereas the summer counterpart showed statistical insignificance in all points. Similar spatial distribution to that shown here is seen in [22] where relatively low *Tm* trends are seen in the west around Cote d'Ivoire and Southwestern Nigeria.

Noticeably, points previously reported for perennial flooding such as the Mahin mud coast around Ayetoro, Nigeria [8], P22–P25 showed a very high rate of increasing extreme *Hs* which could likely translate to a more severe frequent flooding in the future. These locations of high rates of increase in *Hs* can be confirmed in Figure 3 which shows the *Hs* trend and its significance. This same high rate is observed for the P31–P46 which covers the Ghana and Cote d'Ivoire coasts where severe floodings and coastal erosions have increased over the years [41,64]. This can be linked to the already established rising sea level by previous studies such as [8,57], and the reported increase in wave height in the region. When the rate of change in *Hs* for each location during the summer was compared with those of annual and winter trends, an interesting observation was made. It was observed that locations with very low positive trend values during winter and for the annual analysis around Cameroon–Equatorial Guinea (P4–P13) have the highest rates of decrease in the summer. This suggests a possible inverse relationship, where an increase in the winter corresponds to a decrease in the summer. Similar to what is found here, other studies around the world that assessed trends in extreme *Hs* also found a higher positive trend in winter (e.g., [65–68].

Another region of concern is the coastal areas of the Benin Republic and Togo between P25–P31 where high seasonal fluctuation in wave direction has been found. It is worthy of mention that despite most locations showing statistical insignificance for the *Dm* in Figure 7, P29 around Lomé in this region of high seasonal fluctuation showed statistical significance. According to [69], significant accretion and erosion can result from these seasonal changes in average wave direction. This seemingly insignificant change in wave direction has been projected to lead to coastal area land loss of approximately 15–20 ha/year by [46] when coupled with other human interventions such as ports and jetties in the GoG. Additionally, in an assessment of the response of the Bight of Benin, a part of the GoG, to anthropogenic and natural forcing by [57], a similar deduction was made. [57] noted that even a slight change in wave energy and wave incidence angle in the GoG will contribute to the attenuation of transport gradients in the region since they are interdependent. The danger is that either coastal erosion or accretion can occur depending on which of the two is dominant during the period with the highest wave energy. In the GoG, the summer is known to be the high wave energy season and therefore the season in which most of the projected wave impacts will be felt. This fluctuation in wave direction has also been reported to cause beach rotation events from a short timescale (storm duration) to the decadal timescale [69].

5.2. Future Change in Extreme Wave Climate

As noticed in the similarity of the lines for the future time slices under different RCP scenarios, the wave condition is more likely to experience continual changes under any climate change circumstance. This is important in the GoG, especially with the recent rise in the installation of coastal defense systems in countries such as Ghana. Note that the wave climate presented in this study does not take into account the recent coastal engineering developments but just the climate change-driven changes. Hence, a little change in the wave climate due to climate change may show different trend when future studies take into account these features in setting up regional wave models. This is especially important for the wave direction in the GoG as studies have found similar impacts from the construction of major ports such as the Lomé, Abidjan, and Cotonou [46]. Consequently, this little disturbance has led to offsetting the morphodynamic equilibrium previously known in the historically stable GoG. [49,50] reported significant differences between the projected trend of mean and extreme wave conditions which is why it is important not to hastily

conclude that the projected change in mean wave conditions is the same for extremes globally. This may cause misrepresentation of wave climate, especially when applied to the design of marine and coastal structures as well as in the assessment of coastal environmental problems such as flooding and erosion. This understanding of the actual regional changes in extreme wave climate is particularly important for the Ghanaian coast where several coastal defense projects are being implemented to reduce the rates of loss of the coastal communities to coastal erosion and flooding [21]. Other coastal projects noted to be exposed to the impacts of these changes include the Eko Atlantic land reclamation in Lagos, Nigeria [57]. This is very important for the changes in wave direction trend found in this study with an anticlockwise shift in the past to a clockwise shift by the end of the century. Changes in wave direction higher than 1° projected under RCP 8.5 reaffirms the severity of the impacts of climate change in exacerbating coastal erosions and flooding even in places where they were not experienced in the past due to changes in wave direction [70,71]. Of particular interest is the Benin–Togo coastal area where a high change in wave direction up to a 10° clockwise shift is projected. This also happens to be the region where a local significance was found for the change in wave direction as shown in Figure 7. Another reason for concern is the high seasonal fluctuation of the wave direction in this area too. The annual average *Dm* change value greater than 5° has the lowest deviation in the summer of approximately 2° which peaked at almost 10° in the winter. This is noteworthy because this coastal area happens to be one of the locations where the highest change in *Hs* is projected to occur in the future. Hence, close observation of this situation is important to monitor the evolution of these changes. These observations are interesting because Cotonou in Benin was found to be experiencing erosion at a rate of 7.3 m/yr losing about 212 m of the coast between 1979–2012 according to [45]. Going by the future projections for the Benin–Togo coastal part of the GoG, this issue of coastal erosion is likely to get worse if not monitored and properly managed. According to [72], as a result of the large longshore sediment transport rates in the GoG, small deviations in wave–shoreline gradients can cause serious local changes in sediment distribution of either erosion or accretion.

The findings in this study are consistent with the results presented by [49,50] for the tropical and equatorial regions of the North Atlantic Ocean where they projected weak increasing trends in extreme *Hs*. Worthy of note is also the increasingly positive trend of *Hs* from the average to extreme wave conditions which means that the extreme of *Hs* will experience higher rates of increase than the average in the future as shown in Figure 3. According to [70], an increase in *Hs* of about 3% should be expected by the end of the century in the GoG region which agrees with the findings here of 2.04% for RCP 4.5 and 3.4% for RCP 8.5. These values have been estimated as a percentage of the difference between annual mean *Hs* for the past (1979–2005) and the end century (2081–2100).

In the investigation of the Niger Delta wave climate carried out by [36], the result showed decreasing annual and seasonal trends which were described as insignificant. Compared to the findings here, it can be inferred that this will change in the future as the highest change in *Hs* seen between P13–P21 westward signify the significant change from the past to the future in the Niger Delta. Likewise, the Cote d'Ivoire–Ghana regions, which have continued to experience increasing frequency of storm surges and flooding are seen to show a high change in the future too. This implies that wave conditions should be monitored more closely in the westernmost part of the GoG, although serious cases of flooding have been reported even in the eastern part of the Nigerian Transgressive Mud Coast [8]. The impacts of the strengthening of the extra-tropical storm track [73,74] as well as the local trade winds [49] have been linked to the increasing *Hs* in the Southern Hemisphere. The applicability of this impact of the extra-tropical changes in wind conditions in the GoG has been confirmed by [45]. They reported that the equatorial fluctuation of the Inter-Tropical Convergence Zone (ITCZ) is responsible for the variability in local wind waves. The swell waves which are predominant in the GoG correlated with changes in the Southern Annular Mode (SAM) which is an extra-tropical mode in the region of generation

of the swell experienced in the GoG. This is expected to lead to higher swells in the GoG since the Southwestern Atlantic Ocean is the source of the swell experienced in the GoG.

These results for the changes projected for the extreme *Hs* in the GoG seem insignificant in magnitude with maximum change projected to be about a 6% increase by 2100 using RCP 8.5. However, when the predominantly increasing trend in *Hs* is coupled with the severity of sea level rise in most of the low-lying small coastal communities in the GoG, the impacts of the small increase would be seen more inland. This is because the increased water level has extended the reach of the wave action which is the major driver of the coastal erosion in the predominantly sandy beaches in the GoG. Increased wave energy due to the increase in extreme *Hs* in a region previously known for instability in sediment distribution despite low energy requires close monitoring for even small changes.

The results of the trend analysis conducted in this study for the three bulk wave parameters showed average values and trends of the same order of magnitude as those studies at the global and regional scales. For instance, an increasing trend in wave height is reported for most of the global ocean including the tropics where the GoG is located [75]. Though it is noted that wave heights in the tropics are generally lower than in other regions in higher latitudes. Nevertheless, a little change in *Hs* in a relatively unmonitored region can cause serious damage as seen in the increasing frequency of various unexpected storm surges in the case of Cote d'Ivoire in 2011 [37]. This calls for continuous monitoring of the variations in the trends of the wave parameters in the GoG. This is due to the exposure of most of the beaches in the coastal areas in the region thereby increasing their vulnerability to climate change.

In addition to changing storm conditions in the regions of generation of the swell seen in the GoG, other possible contributing factors for the wave condition in the coastal area of the GoG may be a result of the complex interaction of coastline orientation and bathymetry in the region. This theory is supported by the fact that waves at the northwestern coastlines, directly facing the source of waves from the South Atlantic, are higher. This is most likely because they approach the coast unaffected by the bathymetry. Nonetheless, there are little variations in locations with wider continental shelves such as the Volta Delta. Eastward of this unsheltered region lies the Niger Delta, though facing the source of waves too, its wider shelf plays a role in reducing wave energy before reaching the coast. A combination of the sheltering due to the presence of islands such as Sao Tome and Principe as well as Bioko and a wide shelf prevents waves from the South Atlantic from directly coming into the Cameroon–Equatorial Guinea coast. This agrees with findings in other regions such as the Columbia River entrance [76,77], and Aran Islands [77,78].

6. Conclusions

This study has employed the globally available wind wave database containing hindcast for the past (1979–2005) and 21st century forecast for the mid-century (2026–2045) and end-century (2081–2100) under RCP 4.5 and RCP 8.5. In conclusion, the results of this study have confirmed that the impact of climate change on the wave condition in GoG has resulted in increasing trend in yearly and seasonal *Hs*, *Tm* and *Dm*. Significant changes have been seen in the *Hs* in most places in the GoG though few places showed significant change in *Tm* and *Dm*. The projection of more than 1° anticlockwise shift of the wave direction is worthy of close monitoring to ascertain the implications on the resultant longshore drift in the GoG. This changing wave climate has been linked to changes in storms generating these waves offshore and the local effects of changing ITCZ in the region.

This trend may likely increase the frequency and severity of flooding and coastal erosion in various locations along the coast of the GoG, and it is worthy of continuous monitoring into the future. This is because the changing wave direction will likely shift these coastal problems to areas that have not experienced such in the past. The coupled effect of changing wave climate and the increased water level has been on the rise in countries such as Ghana where the severity and frequency of storm surges have become a perennial problem. This close monitoring is very important for the Benin–Togo coast where

high seasonal variabilities in wave climate were seen in the past and are projected to become more significant in the future. Being a region comprised of developing countries with low adaptive and coping capacity, the vulnerability of the coastal dwellers to the impacts of increasing frequency of storm surges is high. This high vulnerability to the impacts of changing wave conditions emphasizes the need to put up an effective monitoring system in form of buoys and early warning systems for the safety of coastal dwellers and users of the ocean and beach resources.

Future works will focus on implementing dynamics wave models for the GoG region to improve the results of wave climate to the coast. This will build on the knowledge of the wave climate currently obtained from statistical downscaling of wave conditions from global wave products. Previous studies including those by [45,57] have made use of globally available databases and relied on empirical modeling due to the large spatial coverage of the GoG region. This large area, coupled with the unavailability of a dedicated regional wave institution, has contributed to the difficulty in providing high-resolution wave data for the region. This limitation has been observed in form of several spatio-temporal non-uniform modeling efforts on local scales in several studies in the region mostly focusing on the northwestern part of the GoG. Success in implementing this regional wave model will be another step closer to understanding the sediment budget of the region and properly managing the coastal issues being faced.

Supplementary Materials: The following supporting information can be downloaded at: https://www.mdpi.com/article/10.3390/jmse10111581/s1. Table S1: Coordinates of selected locations for extreme wave analysis.

Author Contributions: A.M.D.: conceptualization; data curation; methodology; validation; visualization; writing—original draft; writing—review and editing. F.B.: data curation; methodology; software; validation; supervision; writing—reviewing and editing. O.A.D.: conceptualization; methodology; supervision; writing—reviewing and editing. E.B.: resources; project administration; supervision. All authors have read and agreed to the published version of the manuscript.

Funding: This research received no external funding.

Institutional Review Board Statement: Not applicable.

Informed Consent Statement: Not applicable.

Data Availability Statement: The Coordinated Ocean Wave Climate Project phase 2.0 (COWCLIP2.0) wave climate database used in this study is publicly available at https://cowclip.org/data-access/ (accessed on 20 July 2022).

Acknowledgments: This study is performed as part of the DAAD In-Country/In-Region Scholarship Programme for Sub-Saharan Africa at the University of Abomey-Calavi, International Chair in Mathematical Physics and Applications (ICPMA-UNESCO Chair) in Benin Republic. This work is also in the framework of the Jeune Equipe Associée à l'IRD (JEAI) named COASTS UNDER CONTROL by Institut de Recherche pour le Développement (IRD) for their technical support. The authors are grateful to the working group of the second phase of the Coordinated Ocean Wave Climate Project (COWCLIP) (https://cowclip.org (accessed on 20 July 2022)) and the World Climate Research Program (WCRP) in conjunction with the Joint Technical Commission for Oceanography and Marine Meteorology (JCOMM) of the World Meteorological Organization (WMO). Other partnering organizations include the Intergovernmental Oceanographic Commission (IOC) of the United Nations Educational, Scientific Cultural Organization (UNESCO) which powered the public availability of the data used in this study.

Conflicts of Interest: The authors declare no conflict of interest.

References

1. Hemer, M.A.; Trenham, C.E. Evaluation of a CMIP5 derived dynamical global wind wave climate model ensemble. *Ocean Model.* **2016**, *103*, 190–203. [CrossRef]
2. Chowdhury, P.; Behera, M.R.; Reeve, D.E. Wave climate projections along the Indian coast. *Int. J. Clim.* **2019**, *39*, 4531–4542. [CrossRef]

3. Döscher, R.; Acosta, M.; Alessandri, A.; Anthoni, P.; Arneth, A.; Arsouze, T.; Bergmann, T.; Bernadello, R.; Bousetta, S.; Caron, L.-P.; et al. The EC-earth3 Earth system model for the climate model intercomparison project 6. *Geosci. Model Dev. Discuss.* **2021**, *1*, 2021.
4. Kulp, S.A.; Strauss, B.H. New elevation data triple estimates of global vulnerability to sea-level rise and coastal flooding. *Nat. Commun.* **2019**, *10*, 4844. [CrossRef]
5. Sadio, M.; Anthony, E.J.; Diaw, A.T.; Dussouillez, P.; Fleury, J.T.; Kane, A.; Almar, R.; Kestenare, E. Shoreline Changes on the Wave-Influenced Senegal River Delta, West Africa: The Roles of Natural Processes and Human Interventions. *Water* **2017**, *9*, 357. [CrossRef]
6. Mentaschi, L.; Vousdoukas, M.I.; Voukouvalas, E.; Dosio, A.; Feyen, L. Global changes of extreme coastal wave energy fluxes triggered by intensified teleconnection patterns. *Geophys. Res. Lett.* **2017**, *44*, 2416–2426. [CrossRef]
7. Marcos, M.; Rohmer, J.; Vousdoukas, M.I.; Mentaschi, L.; Le Cozannet, G.; Amores, A. Increased Extreme Coastal Water Levels Due to the Combined Action of Storm Surges and Wind Waves. *Geophys. Res. Lett.* **2019**, *46*, 4356–4364. [CrossRef]
8. Dada, O.A.; Almar, R.; Oladapo, M.I. Recent coastal sea-level variations and flooding events in the Nigerian Transgressive Mud coast of Gulf of Guinea. *J. Afr. Earth Sci.* **2019**, *161*, 103668. [CrossRef]
9. Dada, O.A.; Li, G.; Qiao, L.; Ma, Y.; Ding, D.; Xu, J.; Li, P.; Yang, J. Response of wave and coastline evolution to global climate change off the Niger Delta during the past 110 years. *Mar. Syst.* **2016**, *160*, 64–80. [CrossRef]
10. Anthony, E.; Almar, R.; Aagaard, T. Recent shoreline changes in the Volta River delta, West Africa: The roles of natural processes and human impacts. *Afr. J. Aquat. Sci.* **2016**, *41*, 81–87. [CrossRef]
11. Ondoa, G.A.; Bonou, F.; Tomety, F.S.; Du Penhoat, Y.; Perret, C.; Degbe, C.G.E.; Almar, R. Beach Response to Wave Forcing from Event to Inter-Annual Time Scales at Grand Popo, Benin (Gulf of Guinea). *Water* **2017**, *9*, 447. [CrossRef]
12. Morim, J.; Hemer, M.; Cartwright, N.; Strauss, D.; Andutta, F. On the concordance of 21st century wind-wave climate projections. *Glob. Planet. Chang.* **2018**, *167*, 160–171. [CrossRef]
13. Guo, G.; Wang, Y.; Gan, J.; Wu, W.; Ye, Y. Study on wave load prediction and fatigue damage analysis of river-sea-going ship. In Proceedings of the International Conference on Offshore Mechanics and Arctic Engineering, Madrid, Spain, 17–22 June 2018; American Society of Mechanical Engineers: New York, NY, USA, 2018; Volume 51326, p. V11AT12A016.
14. Kamphuis, J.W. *Introduction to Coastal Engineering and management*; World Scientific: Singapore, 2020; Volume 48.
15. McInnes, K.L.; White, C.J.; Haigh, I.D.; Hemer, M.A.; Hoeke, R.K.; Holbrook, N.J.; Kiem, A.S.; Oliver, E.C.J.; Ranasinghe, R.; Walsh, K.J.E.; et al. Natural hazards in Australia: Sea level and coastal extremes. *Clim. Chang.* **2016**, *139*, 69–83. [CrossRef]
16. Shao, M.; Han, Z.; Sun, J.; Xiao, C.; Zhang, S.; Zhao, Y. A review of multi-criteria decision making applications for renewable energy site selection. *Renew. Energy* **2020**, *157*, 377–403. [CrossRef]
17. Smith, G.; Yesilnacar, E.; Jiang, J.; Taylor, C. Marine Habitat Mapping Incorporating Both Derivatives of LiDAR Data and Hydrodynamic Conditions. *J. Mar. Sci. Eng.* **2015**, *3*, 492–508. [CrossRef]
18. Ferreira, A.; Garrido-Amador, P.; Brito, A.C. Disentangling Environmental Drivers of Phytoplankton Biomass off Western Iberia. *Front. Mar. Sci.* **2019**, *6*, 1128. [CrossRef]
19. Nieto, K.; Mélin, F. Variability of chlorophyll-a concentration in the Gulf of Guinea and its relation to physical oceanographic variables. *Prog. Oceanogr.* **2016**, *151*, 97–115. [CrossRef]
20. Abe, J.; Brown, B.E. Towards a Guinea Current Large Marine Ecosystem Commission. *Environ. Dev.* **2020**, *36*, 100590. [CrossRef]
21. Alves, B.; Angnuureng, D.B.; Morand, P.; Almar, R. A review on coastal erosion and flooding risks and best management practices in West Africa: What has been done and should be done. *J. Coast. Conserv.* **2020**, *24*, 1725–1737. [CrossRef]
22. Osinowo, A.; Okogbue, E.; Eresanya, E.; Akande, O. Extreme significant wave height climate in the Gulf of Guinea. *Afr. J. Mar. Sci.* **2018**, *40*, 407–421. [CrossRef]
23. Croitoru, L.; Miranda, J.J.; Sarraf, M. *The Cost of Coastal Zone Degradation in West Africa: Benin, Cote d'Ivoire, Senegal and Togo*; World Bank: Washington, DC, USA, 2019.
24. Grigorieva, V.G.; Badulin, S.I.; Gulev, S.K. Global Validation of SWIM/CFOSAT Wind Waves Against Voluntary Observing Ship Data. *Earth Space Sci.* **2022**, *9*, e2021EA002008. [CrossRef]
25. Vettor, R.; Guedes Soares, C. On the Accuracy of Voluntary Observing Ship's Records. *J. Offshore Mech. Arct. Eng.* **2021**, *143*, 054501. [CrossRef]
26. Vettor, R.; Guedes Soares, C. Comparison of VOS and ERA-Interim Wave Data. In Proceedings of the International Conference on Offshore Mechanics and Arctic Engineering, Glasgow, UK, 9–14 June 2019; American Society of Mechanical Engineers: New York, NY, USA, 2019; Volume 3, p. V003T02A045. [CrossRef]
27. Meucci, A.; Young, I.R.; Breivik, Ø. Wind and Wave Extremes from Atmosphere and Wave Model Ensembles. *J. Clim.* **2018**, *31*, 8819–8842. [CrossRef]
28. Takbash, A.; Young, I.R. Long-Term and Seasonal Trends in Global Wave Height Extremes Derived from ERA-5 Reanalysis Data. *J. Mar. Sci. Eng.* **2020**, *8*, 1015. [CrossRef]
29. Morim, J.; Erikson, L.H.; Hemer, M.; Young, I.; Wang, X.; Mori, N.; Shimura, T.; Stopa, J.; Trenham, C.; Mentaschi, L.; et al. A global ensemble of ocean wave climate statistics from contemporary wave reanalysis and hindcasts. *Sci. Data* **2022**, *9*, 1–8. [CrossRef]
30. Ribal, A.; Young, I.R. 33 years of globally calibrated wave height and wind speed data based on altimeter observations. *Sci. Data* **2019**, *6*, 77. [CrossRef]

31. Vanem, E. Uncertainties in extreme value modelling of wave data in a climate change perspective. *J. Ocean Eng. Mar. Energy* **2015**, *1*, 339–359. [CrossRef]
32. Aarnes, O.J.; Reistad, M.; Breivik, Ø.; Bitner-Gregersen, E.; Ingolf Eide, L.; Gramstad, O.; Magnusson, A.K.; Bent Natvig, B. Projected changes in significant wave height toward the end of the 21st century: Northeast A tlantic. *J. Geophys. Res. Ocean.* **2017**, *122*, 3394–3403. [CrossRef]
33. Perez, J.; Menendez, M.; Mendez, F.; Losada, I.J. Evaluating the performance of CMIP3 and CMIP5 global climate models over the north-east Atlantic region. *Clim. Dyn.* **2014**, *43*, 2663–2680. [CrossRef]
34. Casas-Prat, M.; Sierra, J.P. Projected future wave climate in the NW Mediterranean Sea. *J. Geophys. Res. Ocean.* **2013**, *118*, 3548–3568. [CrossRef]
35. Li, J.; Chen, Y.; Pan, S.; Pan, Y.; Fang, J.; Sowa, D.M. Estimation of mean and extreme waves in the East China Seas. *Appl. Ocean Res.* **2016**, *56*, 35–47. [CrossRef]
36. Osinowo, A.A.; Popoola, S.O. Long-term spatio-temporal trends in extreme wave events in the Niger delta coastlines. *Cont. Shelf Res.* **2021**, *224*, 104471. [CrossRef]
37. Toualy, E.; Aman, A.; Koffi, P.; Marin, F.; Wango, T. Ocean swell variability along the northern coast of the Gulf of Guinea. *Afr. J. Mar. Sci.* **2015**, *37*, 353–361. [CrossRef]
38. Hemer, M.A.; Wang, X.L.; Weisse, R.; Swail, V.R. Advancing wind-waves climate science: The COWCLIP project. *Bull. Am. Meteorol. Soc.* **2012**, *93*, 791–796. [CrossRef]
39. Morim, J.; Trenham, C.; Hemer, M.; Wang, X.L.; Mori, N.; Casas-Prat, M.; Semedo, A.; Shimura, T.; Ben Timmermans, B.; Camus, P.; et al. A global ensemble of ocean wave climate projections from CMIP5-driven models. *Sci. Data* **2020**, *7*, 1–10. [CrossRef]
40. Semedo, A.; Weisse, R.; Behrens, A.; Sterl, A.; Bengtsson, L.; Günther, H. Projection of Global Wave Climate Change toward the End of the Twenty-First Century. *J. Clim.* **2012**, *26*, 8269–8288. [CrossRef]
41. Angnuureng, D.B.; Almar, R.; Senechal, N.; Castelle, B.; Addo, K.A.; Marieu, V.; Ranasinghe, R. Shoreline resilience to individual storms and storm clusters on a meso-macrotidal barred beach. *Geomorphology* **2017**, *290*, 265–276. [CrossRef]
42. Dada, O.A.; Agbaje, A.O.; Adesina, R.B.; Asiwaju-Bello, Y.A. Effect of coastal land use change on coastline dynamics along the Nigerian Transgressive Mahin mud coast. *Ocean Coast. Manag.* **2018**, *168*, 251–264. [CrossRef]
43. Abessolo, G.O.; Hoan, L.X.; Larson, M.; Almar, R. Modeling the Bight of Benin (Gulf of Guinea, West Africa) coastline response to natural and anthropogenic forcing. *Reg. Stud. Mar. Sci.* **2021**, *48*, 101995. [CrossRef]
44. Miller, M.J.; Robinet, T. Life history and morphology of Eel Larvae in the Gulf of Guinea of western Africa: Revisiting Jacques Blache's research (1960–1977) 40 years later. *Rev. Fish Biol. Fish.* **2018**, *28*, 355–379. [CrossRef]
45. Almar, R.; Kestenare, E.; Reyns, J.; Jouanno, J.; Anthony, E.; Laibi, R.; Hemer, M.; Du Penhoat, Y.; Ranasinghe, R. Response of the Bight of Benin (Gulf of Guinea, West Africa) coastline to anthropogenic and natural forcing, Part1: Wave climate variability and impacts on the longshore sediment transport. *Cont. Shelf Res.* **2015**, *110*, 48–59. [CrossRef]
46. Giardino, A.; Schrijvershof, R.; Nederhoff, C.; De Vroeg, H.; Brière, C.; Tonnon, P.-K.; Caires, S.; Walstra, D.; Sosa, J.; Van Verseveld, W.; et al. A quantitative assessment of human interventions and climate change on the West African sediment budget. *Ocean Coast. Manag.* **2018**, *156*, 249–265. [CrossRef]
47. Laïbi, R.A.; Anthony, E.J.; Almar, R.; Castelle, B.; Senechal, N.; Kestenare, E. Longshore drift cell development on the human-impacted Bight of Benin sand barrier coast, West Africa. *J. Coast. Res.* **2014**, *70*, 78–83. [CrossRef]
48. Hemer, M.; Trenham, C.; Durrant, T.; Greenslade, D. CAWCR Global wind-wave 21st century climate projections. *Commonw. Sci. Ind. Res. Organ. Canberra Aust.* **2015**. [CrossRef]
49. Lobeto, H.; Menendez, M.; Losada, I.J. Future behavior of wind wave extremes due to climate change. *Sci. Rep.* **2021**, *11*, 1–12. [CrossRef]
50. Young, I.R.; Vinoth, J.; Zieger, S.; Babanin, A. Investigation of trends in extreme value wave height and wind speed. *J. Geophys. Res. Earth Surf.* **2012**, *117*. [CrossRef]
51. Change, I.C. The physical science basis. In *Contribution of Working Group I to the Fifth Assessment Report of the Intergovernmental Panel on Climate Change*; IPCC: Geneva, Switzerland, 2013; Volume 1535, p. 2013.
52. Bergsma, E.W.; Almar, R.; Anthony, E.J.; Garlan, T.; Kestenare, E. Wave variability along the world's continental shelves and coasts: Monitoring opportunities from satellite Earth observation. *Adv. Space Res.* **2022**, *69*, 3236–3244. [CrossRef]
53. Greene, C.A.; Thirumalai, K.; Kearney, K.A.; Delgado, J.M.; Schwanghart, W.; Wolfenbarger, N.S.; Thyng, K.M.; Gwyther, D.E.; Gardner, A.S.; Blankenship, D.D. The Climate Data Toolbox for MATLAB. *Geochem. Geophys. Geosystems* **2019**, *20*, 3774–3781. [CrossRef]
54. Aydoğan, B.; Ayat, B. Spatial variability of long-term trends of significant wave heights in the Black Sea. *Appl. Ocean Res.* **2018**, *79*, 20–35. [CrossRef]
55. Caloiero, T.; Aristodemo, F.; Ferraro, D.A. Trend analysis of significant wave height and energy period in southern Italy. *Arch. Meteorol. Geophys. Bioclimatol. Ser. B* **2019**, *138*, 917–930. [CrossRef]
56. Wang, J.; Liu, J.; Wang, Y.; Liao, Z.; Sun, P. Spatiotemporal variations and extreme value analysis of significant wave height in the South China Sea based on 71-year long ERA5 wave reanalysis. *Appl. Ocean Res.* **2021**, *113*, 102750. [CrossRef]
57. Anthony, E.; Almar, R.; Besset, M.; Reyns, J.; Laibi, R.; Ranasinghe, R.; Ondoa, G.A.; Vacchi, M. Response of the Bight of Benin (Gulf of Guinea, West Africa) coastline to anthropogenic and natural forcing, Part 2: Sources and patterns of sediment supply, sediment cells, and recent shoreline change. *Cont. Shelf Res.* **2018**, *173*, 93–103. [CrossRef]

58. Osinowo, A.A.; Balogun, I.A.; Eresanya, E.O. Assessment of wave energy resource in the mid-Atlantic based on 37-year numerical hindcast data. *Model. Earth Syst. Environ.* **2018**, *4*, 935–959. [CrossRef]
59. Xorse, T.M. Impact of Wave Dynamics on the Coast of Ghana. Ph.D. Thesis, University of Ghana, Accra, Ghana, 2013.
60. Roest, L.W.M. The Coastal System of the Volta Delta, Ghana. Master's Thesis, Delft University of Technology, Delft, The Netherlands, 2018.
61. Bolle, A.; Das Neves, L.; Rooseleer, J. Coastal protection for Ada, Ghana: A case study. *Proc. Inst. Civ. Eng. Marit. Eng.* **2015**, *168*, 125–133. [CrossRef]
62. Ondoa, G.A.; Onguéné, R.; Eyango, M.T.; Duhaut, T.; Mama, C.; Angnuureng, D.B.; Almar, R. Assessment of the Evolution of Cameroon Coastline: An Overview from 1986 to 2015. *J. Coast. Res.* **2018**, *81*, 122–129. [CrossRef]
63. Kengap, A.K.; Kamga, F.T.; Kwetche, P.F.; Ngueguim, J.R.; Atem, W.E.; Essome, L.M.; Ntangyong, I.L. Impact of hydrodynamic forcings on the morphodynamics of Idenau beach, Western Cameroon coast. *J. Mater. Environ. Sci.* **2020**, *11*, 486–498.
64. Angnuureng, D.; Brempong, K.; Jayson-Quashigah, P.; Dada, O.; Akuoko, S.; Frimpomaa, J.; Mattah, P.; Almar, R. Satellite, drone and video camera multi-platform monitoring of coastal erosion at an engineered pocket beach: A showcase for coastal management at Elmina Bay, Ghana (West Africa). *Reg. Stud. Mar. Sci.* **2022**, *53*, 102437. [CrossRef]
65. Wang, X.L.; Swail, V.R. Changes of Extreme Wave Heights in Northern Hemisphere Oceans and Related Atmospheric Circulation Regimes. *J. Clim.* **2001**, *14*, 2204–2221. [CrossRef]
66. Wang, X.L.; Swail, V.R. Trends of Atlantic Wave Extremes as Simulated in a 40-Yr Wave Hindcast Using Kinematically Reanalyzed Wind Fields. *J. Clim.* **2002**, *15*, 1020–1035. [CrossRef]
67. Caires, S.; Sterl, A. 100-Year Return Value Estimates for Ocean Wind Speed and Significant Wave Height from the ERA-40 Data. *J. Clim.* **2005**, *18*, 1032–1048. [CrossRef]
68. Bricheno, L.M.; Wolf, J. Future wave conditions of Europe, in response to high-end climate change scenarios. *J. Geophys. Res. Ocean.* **2018**, *123*, 8762–8791. [CrossRef]
69. Wiggins, M.; Scott, T.; Masselink, G.; Russell, P.; Valiente, N.G. Regionally-Coherent Embayment Rotation: Behavioural Response to Bi-Directional Waves and Atmospheric Forcing. *J. Mar. Sci. Eng.* **2019**, *7*, 116. [CrossRef]
70. Hemer, M.; Fan, Y.; Mori, N.; Semedo, Á.; Wang, X.L. Projected changes in wave climate from a multi-model ensemble. *Nat. Clim. Chang.* **2013**, *3*, 471–476. [CrossRef]
71. AIT, S.T.; Weesakul, S.; Dastgheib, A.; Ranasinghe, R. *Climate Change Driven Variations in Future Longshore Sediment Transport Rates along the Coast of Vietnam*; Institute of Water Education: Delft, The Netherlands, 2014.
72. Almar, R.; Kestenare, E.; Boucharel, J. On the key influence of remote climate variability from Tropical Cyclones, North and South Atlantic mid-latitude storms on the Senegalese coast (West Africa). *Environ. Res. Commun.* **2019**, *1*, 071001. [CrossRef]
73. Yin, J.H. A consistent poleward shift of the storm tracks in simulations of 21st century climate. *Geophys. Res. Lett.* **2005**, *32*, L18701. [CrossRef]
74. Chang, E.K.M.; Guo, Y.; Xia, X. CMIP5 multimodel ensemble projection of storm track change under global warming. *J. Geophys. Res. Earth Surf.* **2012**, *117*, D23. [CrossRef]
75. Young, I.R.; Zieger, S.; Babanin, A.V. Global Trends in Wind Speed and Wave Height. *Science* **2011**, *332*, 451–455. [CrossRef]
76. Gonazález, F.I. A Case Study of Wave–Current–Bathymetry Interactions at the Columbia River Entrance. *J. Phys. Oceanogr.* **1984**, *14*, 1065–1078. [CrossRef]
77. Herterich, J.G.; Dias, F. Extreme long waves over a varying bathymetry. *J. Fluid Mech.* **2019**, *878*, 481–501. [CrossRef]
78. Herterich, J.G.; Dias, F. Wave breaking and runup of long waves approaching a cliff over a variable bathymetry. *Procedia IUTAM* **2017**, *25*, 18–27. [CrossRef]